SPATIAL AND TEMPORAL STABILITY CHARTS FOR THE FALKNER-SKAN BOUNDARY-LAYER PROFILES

by

A.R. Wazzan, T.T. Okamura, and A.M.O. Smith

REPORT NO. DAC-67086

1 SEPTEMBER 1968

THIS REPORT SUMMARIZES WORK PERFORMED AT THE AIRCRAFT DIVISION UNDER SPONSORSHIP OF THE INDEPENDENT RESEARCH AND DEVELOPMENT PROGRAM OF DOUGLAS AIRCRAFT COMPANY

MCDONNELL DOUGLAS

SPATIAL AND TEMPORAL STABILITY CHARTS FOR THE FALKNER-SKAN BOUNDARY-LAYER PROFILES

by

A.R. Wazzan, T.T. Okamura, and A.M.O. Smith

REPORT NO. DAC-67086

1 SEPTEMBER 1968

THIS REPORT SUMMARIZES WORK PERFORMED AT
THE AIRCRAFT DIVISION UNDER SPONSORSHIP OF
THE INDEPENDENT RESEARCH AND DEVELOPMENT
PROGRAM OF DOUGLAS AIRCRAFT COMPANY

1.0 SUMMARY

The spatial stability of fourteen Falkner-Skan similarity profiles for the range $\beta = -0.1988$ (separation) to $\beta = 1.0$ (stagnation flow) are considered. The Orr-Sommerfeld equation that governs the amplitude of Tollmien-Schlichting disturbances superimposed on flows having such profiles is solved by a step-by-step integration method. The rapid error buildup usually inherent in such methods is eliminated by the use of the Gram-Schmidt orthogonalization procedure. Eigenvalue solutions for values of Reynolds number R_{δ^*} up to 10^5 were successfully obtained for all the cases considered. Curves of constant spatial amplification are presented on the dimensionless frequency vs. Reynolds number diagram for the various β's. The corresponding temporal amplification rates are presented in the form of curves of constant c_i on the dimensionless wave number vs. Reynolds number diagram (curves of constant phase speed c_r are also included). The critical Reynolds number, which is presented as a function of β, is found to be in fair agreement with Pretsch's results. In the present study, however, the separation profile is found to possess a finite critical Reynolds number. Eigenfunction solutions obtained from the present analysis are in excellent agreement with the calculations of Kadbill and Kaplan and also with the experimental data of Schubauer and Skramstad.

2.0 TABLE OF CONTENTS

3.0 INDEX OF FIGURES

4.0 NOMENCLATURE

a_0, a_1, a_2	coefficient of planar fit used to locate zeroes of secular equation (see equation (18))
A	Gram-Schmidt orthogonalization constant defined by equation (11)
c	dimensionless complex velocity of Tollmien-Schlichting disturbance, c_*/U_e
c_g	dimensionless group velocity, c_{g_*}/U_e
F	dimensionless stream function of mean flow
G	characteristic function defined by equation (6)
K	Gram-Schmidt normalization factor for $\bar{\phi}_j$ at y_k
R	Reynolds number based on boundary-layer thickness, $U_e\delta/\nu$
R_{δ^*}	Reynolds number based on displacement thickness, $U_e\delta^*/\nu$
S	denotes spatial values
t	dimensionless time parameter, t_*U_e/δ
T	denotes temporal values
u'	root-mean-square value of longitudinal component of disturbance velocity
U	dimensionless longitudinal velocity component of the mean flow, U_*/U_e
U_e	longitudinal velocity component in the external free stream
x	dimensionless distance along body surface, x_*/δ
y	dimensionless normal to surface coordinate, y_*/δ
Z	normal admittance defined by equation (15)
α	dimensional wave number associated with Tollmien-Schlichting disturbance
α_1	dimensional wave number, $\alpha\delta$
β	Hartree β, dimensionless pressure-parameter
γ	latent root, $[\alpha^2 + i\alpha R(1 - c)]^{1/2}$, of the reduced Orr-Sommerfeld equation in outer region

δ	boundary-layer thickness
δ^*	displacement thickness
ν	kinematic-viscosity coefficient
Δ	Laplace operator, $\partial^2/\partial x^2 + \partial^2/\partial y^2$
η	dimensionless coordinate normal to surface
φ	disturbance amplitude function
ϕ	vector function space defined by equation (9)
Φ	eigenfunction solution
ψ	disturbance stream function
ψ_0	stream function of the mean flow
Ψ	total stream function
ζ	vorticity
ω	dimensionless frequency, $\omega_* \nu / U_e^2$
Ω	constraint function defined by equation (30)

SUPERSCRIPTS

$'$	differentiation with respect to coordinate normal to surface
$-$	denotes normalized values

SUBSCRIPTS

i	imaginary part of complex quantity
r	real part of complex quantity
k	value of k-th integration step
w	wall value
*	where there may be doubt, dimensional quantities are indicated by $(\ )_*$

5.0 INTRODUCTION

The stability of a family of incompressible boundary-layer profiles with respect to disturbances of the Tollmien-Schlichting type has been extensively treated by only two people, Schlichting[1] and Pretsch[2]. Schlichting analyzed the Pohlhausen family and Pretsch the Falkner-Skan family. The profiles of the Pohlhausen family are convenient for analysis but, of course, are only approximations of the exact solutions. The profiles of the Falkner-Skan family, which are exact solutions, are considered in this report. The velocity profiles that occur in this family, such as $\beta = 0$ (flat-plate flow), $\beta = -0.1988$ (separation), and $\beta = 1.0$ (stagnation flow), are of practical as well as theoretical interest. It was for a flow over a flat plate that Schubauer and Skramstad first demonstrated the occurrence of the theoretically predicted regions of instability as the first step in the transition process from laminar to turbulent flow. The connection between instability and transition is still largely unresolved. Nonetheless, a semiempirical method for predicting transition developed independently by Smith[3] and Van Ingen[4] enjoyed remarkable success. The theoretical analyses for all these important papers were based on the stability characteristics of the Falkner-Skan profiles.

The stability of Falkner-Skan profiles is reconsidered here because the earlier works by both Schlichting and Pretsch involve approximate representation of the mean flow and rely on asymptotic methods to obtain solutions of the stability equation. It has since been found that asymptotic methods, although useful in establishing conditions for stability at high Reynolds numbers, often lack accuracy at lower Reynolds numbers[5]. Moreover, because of the presence of the second derivative of the mean velocity in the stability equation, it is important to use accurate velocity profiles in performing stability calculations. The different results obtained by Schlichting and Pretsch for a flow in the presence of an adverse pressure gradient serve to demonstrate this point. In this situation, the upper branch of the neutral curve approaches an asymptote, $\alpha_r \delta^* = \text{constant}$, as $R_{\delta^*} \to \infty$. For the separating profile ($\beta = -0.1988$) the difference in the numerical values obtained was considerable. Schlichting obtained 0.450, whereas Pretsch obtained 1.07. This difference is primarily due to the assumed form of the mean velocity profile. Schlichting based his solution on a polynomial

approximation of the velocity profile. Pretsch based his on the more accurate profile calculated by Hartree[6]. With the exception of a few cases (mainly $\beta = 0$ for a limited range of Reynolds number), the mathematical difficulties encountered in the stability analysis have discouraged further attempts to improve the stability charts produced by these early investigators. The usefulness of the charts and a desire to devise the mathematical techniques necessary to treat this and similar problems efficiently prompted a further investigation into the stability properties of these profiles.

Because of the limitations of asymptotic analytic methods, there has been a considerable effort devoted in recent years to the development of numerical methods. These inherently afford good accuracy at low Reynolds numbers but encounter numerical difficulties at high values. A notable advance was made by Landahl and Kaplan[7] with their "purification scheme". It cleverly circumvents the rapid error buildup that usually occurs in the step-by-step integration of the Orr-Sommerfeld equation. This equation is commonly accepted as the basis for stability investigations in two-dimensional incompressible isothermal flows. The purification scheme was found adequate to deal with cases in which the Reynolds number based on boundary-layer thickness did not exceed 10^4. In many practical cases, critical Reynolds numbers far greater than 10^4 must be considered. For example, in flows with adverse pressure gradients, the asymptotic behavior of the neutral curve is established at very large Reynolds numbers. The Reynolds number restriction thus imposes a severe limitation on the class of problems that can be investigated by Landahl and Kaplan's method. Nonetheless, their basic approach is sound and the more precise mathematical formulation of the "purification" procedure adopted in the present analysis has proved successful in eliminating the shortcoming.

In the present investigation the purification scheme of Landahl and Kaplan is replaced by the Gram-Schmidt orthogonalization procedure[8]. This innovation has been successfully applied to the solution of the Orr-Sommerfeld equation for values of Reynolds numbers R_{δ^*} up to 10^5. The velocity profiles used to perform the stability calculations are obtained from a direct numerical integration of the boundary-layer equation.

6.0 ANALYSIS

6.1 The Orr-Sommerfeld Equation

The dynamic equation for an incompressible, non-heat-conducting, viscous fluid in two-dimensional parallel flow written in terms of the vorticity $\zeta(t,x,y)$ and stream function $\Psi(t,x,y)$ is

$$\frac{\partial \zeta}{\partial t} = \frac{i}{R}\Delta\zeta + \frac{\partial \Psi}{\partial x}\frac{\partial \zeta}{\partial y} - \frac{\partial \Psi}{\partial y}\cdot\frac{\partial \zeta}{\partial x} \tag{1a}$$

where

$$\zeta = \Delta\Psi \tag{1b}$$

The above equations have been made dimensionless by normalizing all lengths by the reference length δ, all velocities with respect to U_e, and all times by δ/U_e. For the purpose of linearization, a small disturbance $\psi(x,y,t)$ is superimposed on the mean flow ψ_0; i.e.,

$$\Psi = \psi_0(y) + \psi(x,y,t) \tag{2}$$

Introduction of the Tollmien-Schlichting wave

$$\psi = \varphi(y)e^{i\alpha_1(x-ct)} \tag{3}$$

into equation (2) and substituting the resulting stream function into equation (1a) leads, after linearization, to the familiar Orr-Sommerfeld equation (hereafter referred to as the O-S equation),

$$(U - c)(\varphi'' - \alpha_1^2\varphi) - U''\varphi = -\frac{i}{\alpha_1 R}(\varphi'''' - 2\alpha_1^2\varphi'' + \alpha_1^4\varphi) \tag{4}$$

Henceforth subscript 1 on α is deleted for convenience. The boundary conditions assumed for the present problem are homogeneous. Thus the solution of the O-S equation constitutes an eigenvalue problem leading to the solution of a secular equation of the form $G(R, \alpha, c) = 0$.

6.2 Spatial Amplification of Disturbance

Traditionally, in the formulation of the eigenvalue problem disturbances are considered as amplified or damped in time; α is taken to be real $(\alpha = \alpha_r)$ and the frequency $\omega = \alpha c$ is taken to be complex $(\omega = \omega_r + i\omega_i)$. The temporal point of view is of course ideal for such analysis. This becomes obvious when we note that in the governing equations of motion, the temporal derivatives are of first order and have a coefficient of unity, whereas the other derivatives, all of the spatial variety, are of higher order and appear in more complicated forms. The temporal viewpoint has produced theoretical predictions that are, in some cases, in fair agreement with experimental observations. Much of the discussion that follows in this section may be found in the current literature (e.g., reference 7), but will be presented here for the sake of completeness.

Physical observations of the breakdown of laminar flows in a boundary layer have revealed the presence of combined spatial and temporal growth of small wavelike disturbances preceding transition, e.g., Brown[9]. On the other hand, the forced-oscillation experiments of Schubauer and Skramstad[10] and Klebanoff, Tidstrom, and Sargent[11] give illustrations of a purely spatial growth of disturbances. These observations necessitate a closer look into the adequacy of the description of the growth of small disturbances as a process of temporal amplification. In this paper the eigenvalue problem for the case of spatial amplification, $G(\alpha_{complex}, \omega_{real}) = 0$, is considered. Two different approaches for bridging the difference between the theoretical and the observed descriptions of the phenomenon will be discussed. The first is described in a note by Gaster[12] that derives a relation between the spatial and temporal amplification rates under the assumption that these rates are small. The transformation states that to the order of ω_{im}^2, where ω_{im} is the maximum value of ω_i at a given Reynolds number, one may write

$$\alpha_i(S) = -\frac{\alpha c_i(T)}{c_g} + O(c_i^2) \tag{5a}$$

$$\alpha_r(S) = \alpha(T) \tag{5b}$$

$$\omega_r(S) = \omega_r(T) \tag{5c}$$

where the disturbance group velocity c_g is given by

$$c_g = c_r + \alpha \frac{\partial c_r}{\partial \alpha} = \frac{\partial(\alpha c_r)}{\partial \alpha} = \frac{\partial \omega_r}{\partial \alpha_r} \tag{5d}$$

and S and T denote spatial and temporal systems, respectively. Note that the group velocity of a dispersive wave system is the speed at which the energy of the disturbance is convected. For fixed-frequency disturbances, one must recognize that although αc_r is fixed, its variation with wave number does not vanish and that energy may still be carried by a disturbance at a velocity different from its phase speed. The method is based on the linearization of the relationship between α and c in any given neighborhood. This method of relating spatial and temporal amplification rates was used by Landahl and Kaplan[7] in studying the stability of laminar flow over compliant boundaries. Recently, however, Betchov and Criminale[13] showed that the linear relationship between α and c assumed by Gaster is not always valid in regions away from the neutral curve. In fact, there may be regions for which the temporal criterion does not predict instability although the spatial criterion does.

The other approach to spatial amplification is of course the direct attack on the characteristic equation,

$$G(\alpha, \omega, R) = 0 \tag{6}$$

by regarding α as a complex parameter and considering only real values for ω, thus restricting c to be proportional to the complex conjugate of α. In this approach, which is used in the present investigation, there is no restriction on the magnitudes of α and c, as there is with Gaster's transformation.

It must be noted that a complex α introduces amplifications of the form $e^{-\alpha_i x}$. A term of this form causes exponential growth of the disturbances for either positive or negative x for the case of nonzero α_i. Thus, to develop a stability criterion, one must determine whether the disturbances grow as they travel in the upstream or downstream direction. Establishing a criterion for spatial stability requires knowledge of the direction in which the wave is amplified and of the direction in which energy is carried by the disturbance, as determined by the sign of the group velocity. The spatial criterion for stability is presented in table I. The temporal criterion for stability is also presented for comparison. The use of the group velocity in the stability

Table I

SPATIAL AND TEMPORAL CRITERION OF STABILITY ACCORDING TO LANDAHL AND KAPLAN[9]

Temporal Growth	Spatial Growth	Stability
$c_i > 0$	$\alpha_i < 0$ $c_g > 0$	Unstable
	$\alpha_i > 0$ $c_g < 0$	
$c_i = 0$	$\alpha_i = 0$	Neutral
$c_i < 0$	$\alpha_i > 0$ $c_g > 0$	Stable
	$\alpha_i < 0$ $c_g < 0$	

criterion for spatial growth of disturbances is an effective application of a radiation condition. Hence, disturbances are unstable as they convect energy in the same direction as that of their spatial growth. By means of Gaster's transformations, equation (5), it is seen from table I that the two criteria, the spatial and the temporal, are consistent. The present paper reports on the spatial stability of Falkner-Skan similarity profiles for which the characteristic function is solved in terms of real values of ω and complex values of α.

6.3 Solution of the Orr-Sommerfeld Equation

When the coefficients of the O-S equation vary in the range of interest, as in the present case, no closed-form solution exists. In the region outside the boundary layer, the mean flow is constant and the O-S equation reduces to the following equation with constant coefficients:

$$\varphi'''' - (\alpha^2 + \gamma^2)\varphi'' + \alpha^2\gamma^2\varphi = 0 \tag{7}$$

where $\gamma^2 = \alpha^2 + i\alpha R(1 - c)$. This differential equation has four solutions expressible in terms of exponential functions, as follows

$$\varphi_1 = e^{-\alpha y} \qquad \varphi_2 = e^{\alpha y}$$

$$\varphi_3 = e^{-\gamma y} \qquad \varphi_4 = e^{\gamma y} \tag{8}$$

where the real parts of α and γ are greater than zero. If the solutions are to remain bounded as $y \to \infty$, then φ_1 and φ_3 are the only admissible solutions. Since φ_1 and φ_3 satisfy the O-S equation at the outer edge of the boundary layer (i.e., $y = 1$), they are used to specify initial conditions for the corresponding solutions within the boundary layer itself. A Runge-Kutta method for a fourth-order differential equation is used to integrate the O-S equation with the parameters R and α fixed. A linear combination of these two solutions is then formed to satisfy a boundary constraint at the wall. A numerical search procedure is then used whereby the value of the parameter α is found for which the boundary conditions at the wall are satisfied. The particular values of R, α, and c for which this is true are referred to as eigenvalues. The problem is thus solved, at least in principle. In practice, however, two solutions that are linearly independent at the beginning of the integration are observed to become linearly dependent within the region of interest. This difficulty can be removed by using multiple-precision arithmetic, which is rather costly in terms of programmer and computer time.

6.4 Gram-Schmidt Orthogonalization Procedure

Initially, at least, the two solutions φ_1 and φ_3 are linearly independent. To insure that they remain so, the following function space is defined:

$$\phi(y) = (\varphi,\ \varphi',\ \varphi'',\ \varphi''') \tag{9}$$

A given vector in this complex function space completely defines a solution of the governing equation. Two solutions or, equivalently, two vectors in this function space that are linearly independent (noncollinear) may be linearly combined to construct another solution (vector) that is entirely free of any one of the generating solutions (vector). Because of round-off, ϕ_1 has a small parasitic error proportional to ϕ_3. To remove the parasitic error from the integrated solution, an auxiliary function $\tilde{\phi}_1$ is constructed such that no component of ϕ_3 is contained in it. This is accomplished by normalizing the integrated values of ϕ_3 at the end of each step of the integration and constructing, at some y_k, the function $\tilde{\phi}_1$, as follows:

$$\tilde{\phi}_1(y_k) = \phi_1(y_k) - A\bar{\phi}_3(y_k) \tag{10}$$

where $\bar{\phi}_3$ is the normalized value and A is an as yet undetermined constant. Since it is desired to remove any presence of the solution $\bar{\phi}_3$ from $\tilde{\phi}_1$, the function $\tilde{\phi}_1$ is constructed to be orthogonal to $\bar{\phi}_3$. Hence,

$$A = \phi_1(y_k) \cdot \bar{\phi}_3(y_k) \tag{11}$$

and

$$\tilde{\phi}_1 = \phi_1(y) - \left[\phi_1(y_k) \cdot \bar{\phi}_3(y_k)\right] \bar{\phi}_3(y) \tag{12}$$

Since ϕ_1 and ϕ_3 represent solutions of the O-S equation, the purified solution $\tilde{\phi}_1$ is also a solution. The procedure may be extended to generate additional independent solutions as desired. The algorithm is known as the Gram-Schmidt orthogonalization procedure.

The purification of the integrated solution for ϕ_1 may be applied at any arbitrary step of the integration, provided the solution has not become completely dominated by the parasitic error. In the present study the orthogonalization procedure is applied at each step of the integration. No investigation was made to determine the effect of the frequency of orthonormalization on the results. The above method is used in conjunction with the integration (IBM 7094) of the O-S equation for a number of Falkner-Skan velocity profiles. Single-precision arithmetic was adequate for all the necessary computations in the stability analysis.

6.5 Numerical Determination of the Eigenvalue Criterion

To solve the eigenvalue problem numerically, one does not need to know the functions $\tilde{\phi}_1(y)$ and $\bar{\phi}_3(y)$, but only their values at the wall. A solution Φ is constructed as follows:

$$\Phi = \tilde{\phi}_1 + B\bar{\phi}_3 \tag{13}$$

where B is selected from the requirement that

$$c\Phi'_w + D\Phi_w = 0 \tag{14}$$

and D is some arbitrary constant. The boundary-layer admittance Z, which is proportional to ϕ_w, is substituted for the boundary condition $\Phi_w = 0$

$$Z(R, \alpha c, \alpha) = \frac{-\alpha^2 R\Phi_w}{\Phi'''_w - \alpha^2\Phi'_w} \tag{15}$$

The eigenvalue criterion is then the condition that Z vanishes. When this occurs,

$$\Phi_w = \Phi'_w = 0 \tag{16}$$

and the boundary conditions at the wall are satisfied. The quantity Z is, in general, complex. Hence, equation (15) may be expressed separately in terms of

its real and imaginary components, thus yielding two equations in two unknowns. There are only two unknowns, since R and αc are held fixed and α is taken to be a complex number. Thus equation (15) may be written in the functional form

$$Z_r = Z_r(\alpha_r, \alpha_i)$$

$$Z_i = Z_i(\alpha_r, \alpha_i) \tag{17}$$

The application of a standard iteration method to solve these equations is convenient. However, because of the acute sensitivity of the topology of Z to small changes in α, such a scheme is inadequate to meet the general requirements of the problem. The use of a LaGrange-type interpolation such as that employed by Landahl and Kaplan proved unsatisfactory for the Reynolds number range considered in this study. The procedure now used is to fit a plane to three successive trial points of the form

$$\alpha = a_0 + a_1 Z_r + a_2 Z_i \tag{18}$$

where the a's are, in general, complex. The first two trials are based on either estimates or extrapolations of previously established eigenvalues for fixed R's and αc's. The third is obtained from a linear prediction based on the first two. Thereafter, the aforementioned procedure is used. The value for α in the next trial is simply a_0. It is given by the equation

$$a_0 = \frac{\left(Z_{r_2} Z_{i_3} - Z_{r_3} Z_{i_2}\right)\alpha_1 + \left(Z_{r_3} Z_{i_1} - Z_{r_1} Z_{i_3}\right)\alpha_2 + \left(Z_{r_1} Z_{i_2} - Z_{r_2} Z_{i_1}\right)\alpha_3}{\left(Z_{r_2} Z_{i_3} - Z_{r_3} Z_{i_2}\right) + \left(Z_{r_3} Z_{i_1} - Z_{r_1} Z_{i_3}\right) + \left(Z_{r_1} Z_{i_1} - Z_{r_2} Z_{i_1}\right)} \tag{19}$$

Under the present scheme, there is one free parameter that one may fix to modify the topology of the surfaces expressed by equation (17). That parameter is D in equation (14). It was found that setting D equal to U''_w led to satisfactory results for all the cases considered. It is sometimes desirable to select a different set of arguments to solve the characteristic problem. To determine points on a curve of constant temporal amplification

such as, say, the neutral curve $(c_i = 0)$, one may choose α_r and Λ, where Λ is defined by the relation $\Lambda = \alpha_r/c_r$. This procedure was in fact used to generate eigenfunction solutions for neutral disturbances.

6.6 Determination of the Eigenfunction

Once the eigenvalues are found, the task of constructing the corresponding eigenfunction is relatively simple. The two solutions denoted by $\tilde{\phi}_{1,k}(y)$ and $\bar{\phi}_{3,k}(y)$ corresponding to some y_k are related to the previous sets obtained by the Gram-Schmidt orthogonalization procedure by the recursion formulas

$$\bar{\phi}_{3,k} = \bar{\phi}_{3,k-1}\, K_k = \bar{\phi}_{3,k-2}\, K_k\, K_{k-1} \tag{20a}$$

$$= \bar{\phi}_{3,k-m} \prod_{j=0}^{m-1} K_{k-j} \qquad m \geq 1 \tag{20b}$$

and

$$\tilde{\phi}_{1,k} = \tilde{\phi}_{1,k-1} - A_k\, \bar{\phi}_{3,k} \tag{21a}$$

$$= \tilde{\phi}_{1,k-2} - A_k\, \bar{\phi}_{3,k} - A_{k-1}\, \bar{\phi}_{3,k-1} \tag{21b}$$

$$= \tilde{\phi}_{1,k-m} - \sum_{n=0}^{m-1} A_{k-n}\, \bar{\phi}_{3,k-n} \qquad m \geq 1 \tag{21c}$$

The constant K_k is the normalization factor for $\bar{\phi}_{3,k}$ at y_k. In the course of integration, $\tilde{\phi}_{1,k-m}(y)$ and $\bar{\phi}_{3,k-m}(y)$ are evaluated at a single point. These are in fact the quantities $\tilde{\phi}_1(mh)$ and $\bar{\phi}_3(mh)$ defined earlier. Therefore, it is convenient to express equation (21c) in a slightly different form. From equation (20b) it may be shown that

$$\frac{\bar{\phi}_{3,k-n}}{\bar{\phi}_{3,k-m}} = \prod_{j=n}^{m-1} K_{k-j} \qquad m - 1 \geq n \tag{22}$$

so that

$$\tilde{\Phi}_{1,k} = \tilde{\Phi}_{1,k-m} - b_{k,m}\,\bar{\Phi}_{3,k-m} \tag{23}$$

where

$$b_{k,m} = \sum_{n=0}^{m-1} A_{k-n} \prod_{j=n}^{m-1} K_{k-j} \tag{24}$$

Note that

$$b_{k,m+1} = K_{k-m}\,[b_{k,m} + A_{k-m}] \tag{25}$$

The solutions $\tilde{\Phi}_{1,w}(y)$ and $\bar{\Phi}_{3,w}(y)$ may be readily evaluated from the above formulas by simply saving the values of $\tilde{\Phi}_1$, $\bar{\Phi}_3$, A_k, and the normalization factor K_k at each integration step. The eigenfunction is determined by combining equations (13), (20b), and (23) to yield

$$\Phi(mh) = \tilde{\Phi}_1(mh) + \left[B \prod_{j=0}^{m-1} K(jh) - b_{k,m}\right] \bar{\Phi}_3(mh) \tag{26}$$

where

$$b_{k,m} = \sum_{n=0}^{m-1} A(nh) \prod_{j=n}^{m-1} K(jh) \tag{27}$$

6.7 Solution of Velocity Profile of the Mean Flow

The Falkner-Skan profiles are obtained by a numerical integration of the boundary-layer equation

$$F'''(\eta) = -FF'' + \beta(F'^2 - 1) \tag{28}$$

with the appropriate value of β. The boundary conditions for this equation are

$$F(0) = F'(0) = \lim_{\eta \to \infty} (F' - 1) = 0 \tag{29}$$

A family of solutions of equation (28) can be generated by using the initial conditions given by equation (29) and various trial values of $F''(0)$. These solutions may be parametrically represented as functions of η and $F''(0)$. Making use of the asymptotic nature of the desired solution reduces the original two-point boundary-value problem to finding the minimum (zero) of a function Ω given by

$$\Omega[F''(0), \eta] = W_1(F' - 1)^2 + W_2(F'')^2 + W_3(F''')^2 \tag{30}$$

The quantities W_1, W_2, and W_3 are weight factors. Since the boundary condition on $F'(\eta_\infty)$ is explicit, whereas those on $F''(\eta_\infty)$ and $F'''(\eta_\infty)$ are implicit, W_1 was taken as 10 and W_2 and W_3 were taken as unity. The particular form of the constraint relation given by equation (30) was chosen because it is suited for solving boundary-layer problems for which F' is a monotonically increasing function. The process is initiated by using trial values of $F''(0)$ until at least one high and one low value have been obtained. A high or low value is determined by integrating equation (28) until the product $(F' - 1)F''$ becomes positive and then checking the sign of either factor. If it is positive, the value of $F''(0)$ is high; if it is negative, the value of $F''(0)$ is low. Quadratic interpolation is employed to yield $\Omega_{min}[F''(0)]$ equal to zero from the last high and low trials of $F''(0)$. Rapid convergence of this process has been established.

With $F(0)$, $F'(0)$, and $F''(0)$ specified, the solution of equation (28) is treated as an initial-value problem that is solved by a Runge-Kutta method for third-order differential equations. The calculations were made on the 7094 IBM computer with double-precision arithmetic. The profiles obtained are in agreement with Smith's[14], which are tabulated to five decimal places.

The normalized velocity and its second derivative, which appear in the O-S equation, are related to the function F as follows:

$$U(y) = F'(y) \tag{31}$$

and

$$U''(y) = (\eta_\delta)^2 F'''(y) \tag{32}$$

where η_δ is taken to correspond to the point at which the normalized velocity has the value 0.9990. The velocity profiles thus obtained are used to integrate the O-S equation across the boundary layer.

The values obtained for the momentum thickness θ, shape factor H, boundary-layer thickness η_δ, and the displacement thickness Δ^*, are given in table II. The characteristic length used in normalizing the stability parameters is $\delta^* = \Delta^* \sqrt{(2 - \beta)\nu x_*/U_e}$.

Table II

BOUNDARY-LAYER PARAMETERS FOR VARIOUS β's

β	η_δ	$\Delta^* = \int_0^\infty F' d\eta$	$\theta = \int_0^\infty F'(1-F') d\eta$	H
1.0	3.143	0.6479	0.2923	2.216
0.8	3.280	0.6987	0.3119	2.240
0.6	3.440	0.7640	0.3359	2.274
0.5	3.533	0.8046	0.3503	2.297
0.4	3.636	0.8526	0.3667	2.325
0.3	3.752	0.9110	0.3857	2.362
0.2	3.887	0.9842	0.4082	2.411
0.10	4.048	1.0803	0.4355	2.481
0.05	4.145	1.1417	0.4515	2.529
0.0	4.257	1.2168	0.4696	2.591
-0.05	4.390	1.3124	0.4905	2.676
-0.10	4.561	1.4427	0.5150	2.801
-0.14	4.744	1.5459	0.5386	2.963
-0.1988	5.562	2.359	0.5854	4.029

7.0 RESULTS AND DISCUSSION

The results of the present study are presented in the form of curves of constant $\alpha_i \delta^*/R_{\delta^*}$ on the diagrams of dimensionless frequency vs. Reynolds number (ω_r, R_{δ^*}) in figures 1 through 14. The critical Reynolds number $R_{\delta^*_{crit}}$ determined by cross-plotting the computed data is presented as a function of Hartree β's in table III and is shown in figure 15. The Reynolds number at maximum spatial amplification rate is presented as a function of β in figure 16. For purposes of comparison, Pretsch's results (obtained on the basis of temporal considerations) are also given. For the separation profile, Pretsch's results indicate that unstable disturbances are always present, whatever the Reynolds number. This strongly suggests that all separation flows are essentially turbulent. A lower mode, perhaps correspoinding to Pretsch's was in fact discovered in the present analyses. This is shown in figure 31. The wave-number spectrum for this mode is especially small, indicating that insofar as

Table III

CRITICAL REYNOLDS NUMBER FOR VARIOUS β's

β	$R_{\delta^*_{crit}}$	
	Present Analysis	Pretsch
1.0	12490	12600
0.8	10920	
0.6	8890	8300
0.5	7680	
0.4	6230	5000
0.3	4550	
0.2	2830	3200
0.1	1380	
0.05	865	
0.0	520	660
-0.05	318	
-0.10	199	126
-0.14	138	
-0.1988	67	0

stability is concerned the dominant mode is the one possessing the critical Reynolds number $R_{\delta^*} = 67$ shown on the same graph. Unstable disturbances corresponding to the lower mode were found to propagate upstream ($c_g < 0$)! These self-excited oscillations apparently do not lead to transition, at least until a critical Reynolds number is reached, for laminar separation has certainly been experimentally observed. The maximum frequency ω_{max} for which disturbances are unstable, as well as the maximum amplification rate $(-\alpha_i \delta^*/R_{\delta^*})_{max}$, is shown in figure 17.

In order to carry out a more thorough comparison with the results of other investigators, and particularly with those of Pretsch, curves of constant c_i and c_r calculated from the present spatial results are presented on the diagram of dimensionless wave number vs. Reynolds number $(\alpha_r \delta^*, R_{\delta^*})$, figures 18 through 31. The neutral curves are summarized in figure 32. Contours of the neutral curves obtained by Pretsch (not shown) are generally in fair agreement with the present results for positive β's. Pretsch's neutral curve for the Blasius profile encloses a much smaller wave number spectrum for Reynolds numbers near the critical as may be seen in figure 33, in which the predicted maximum wave number for which disturbances are unstable $(\alpha_r \delta^*)_{max}$ is plotted as a function of β. The contour along the lower branch of the neutral curve was found to be in good agreement with the present results. The maximum temporal amplification rate, $c_{i_{max}}$, is also compared in figure 33. Pretsch's results were obtained on the basis of a temporal criterion and the present results on the basis of a spatial criterion. The agreement shown between the results for maximum amplification rates obtained from the two analyses is an indication that the use of the Gaster transformation in connecting the results of the spatial and temporal analyses is valid, at least insofar as unstable disturbances are concerned. The discrepancy between the results of the two analyses is perhaps best explained by the fact that asymptotic methods are less accurate in regions where viscous effects are important. In this region the inviscid solution is less representative of the total solution. The viscous correction is therefore less able to compensate for this defect, particularly at low Reynolds number such as near the critical Reynolds number of a Blasius profile or profiles having an adverse pressure gradient.

In the case of the negative Hartree β's, it has been theoretically established that at large Reynolds numbers the upper branch of the neutral curve does not approach the R_{δ^*}-axis, as it does with positive β's, but

approaches a certain asymptote $\alpha_r \delta^* = \text{constant}$. This result was discussed by Tollmien[15], who showed that the constant is a function of β. The asymptotes for $\alpha_r \delta^*$ for these cases provide a further check on the validity of the present results, because the limiting inviscid solution must emerge as the exact solution of the complete Orr-Sommerfeld equation as $R \to \infty$ for nonzero values of the wave number α. In this region the asymptotic method used by Pretsch should be valid. The comparison in figure 34 for $\beta = -0.10$ shows good agreement with the asymptotic value obtained by Pretsch. It may be noted from figure 28 that the neutral curve for $\beta = -0.05$ obtained from the present analysis had not reached an asymptote even at $R_{\delta^*} = 10^5$. For this reason, the calculations were extended to a Reynolds number of 200,000 for this case. Similar calculations were made for the cases $\beta = -0.01$ and $\beta = -0.025$. In none of these cases was an asymptote firmly established, although the gradient present was found to be small. The values for $R_{\delta^*} = 2 \times 10^5$ are plotted on the figure.

Velocity perturbations for the Blasius profile at $R_{\delta^*} = 902$ and 2080 were obtained by matching the minimal value of the eigenfunction solutions to the experimentally observed amplitudes of Schubauer and Skramstad. These are shown in figures 35 and 36, respectively. From the description given in Schubauer and Skramstad's report, one cannot precisely determine the location in the profile where the measurements were made. To locate a neutral disturbance, the hot wire would have had to be moved several inches downstream in order to get a measurable change in amplitude. As a result, the wire would have had to be moved upward enough to maintain the same similar distance from the surface. This adjustment is physically difficult to accomplish. The point at which phase reversal takes place is more readily established experimentally. This may be done by simply fairing through the available data. The data of Schubauer and Skramstad is rescaled to match the point of phase reversal with the results of the theoretical analysis (shown on same figure). It may be observed in figures 35 and 36 that the correlation with theory is significantly improved in the two cases considered. Of particular note is the much closer agreement obtained for the location of the maximum and minimum within the boundary layer. The solutions obtained by Radbill[16] have also been included in these figures.

The agreement between the results of the theoretical analyses is quite good and is somewhat reassuring, since in the present analysis no investigation into the effect of the frequency of application of the Gram-Schmidt procedure on the eigenfunction solution had been made. The computation time required to establish one set of eigenvalues is roughly 20 seconds. A comparison with Kaplan's result for $R_\delta = 3000$ is shown in figure 37.

8.0 CONCLUDING STATEMENTS

Solutions for Reynolds numbers up to $R_{\delta^*} = 10^5$ were successfully obtained by the present method for all the cases. This Reynolds number is at least 50 times as large as that which can be handled by the "purification" scheme devised by Landahl and Kaplan. The method is capable of being extended into the inviscid region and in fact precludes the necessity for performing an inviscid analysis in most practical situations. It is clear that the present method's capability of coping with the numerical difficulties encountered in performing a stability analysis of small disturbances in an inviscid problem may be adapted to deal with compressible flows.

9.0 ACKNOWLEDGEMENTS

The authors express their gratitude to Professor Richard E. Kaplan, Aerospace Dept., University of Southern California, for his cooperation in the initial phase of this study. In addition, Mr. David Callin is acknowledged for his part in the considerable task of processing the numerical data. Mr. Kalle Kaups is acknowledged for valuable discussion and suggestions.

10.0 REFERENCES

1. Schlichting, H. and Ulrich, A.: On the Calculation of the Transition Laminar/Turbulent. Jahrb (1942) d. DL I p.8.
2. Pretsch, J.: The Stability of a Two-Dimensional Laminar Flow in Pressure Drop and Pressure Rise. Jahrb (1941) d. DL I p.58.
3. Smith, A.M.O.: Transition, Pressure Gradient, and Stability Theory. Proc. 9-th Intern. Congress of Applied Mech., Brussels, Vol. 4, (1957). p.234; see also Report No. ES 26388 of the Douglas Aircraft Co., El Segundo, Calif. (1956).
4. Van Ingen, J.L.: A Suggested Semiempirical Method for the Calculation of the Boundary Layer Transition Region. Dept. Aero. Eng., Inst. of Technology, Delft, Report V.T.H. 74 (1956).
5. Wazzan, A.R.; Okamura, T.T.; and Smith, A.M.O.: The Stability of Laminar Boundary Layers at Separation. The Phys. of Fluids, Vol. 10, No. 12, p.2540 (1967).
6. Hartree, D.R.: On an Equation Occurring in Falkner and Skan's Approximate Treatment of the Equation of the Boundary Layer. Proc. Phil. Soc. Cambridge, Vol. 33, (1937) p.223.
7. Landahl, M.T. and Kaplan, R.E.: The Effect of Compliant Walls on Boundary Layer Stability and Transition. AGARDograph 97, part I, Naples, Italy (1965).
8. Bellman, R.E. and Kalaba, R.E.: Quasilinearization and Nonlinear Boundary Value Problems. American Elsevier Publishing Company, New York, (1965) pp. 98-103.
9. Brown, F.M.N.: Boundary Layer Transition. Dept. of Aero. Engr., University of Notre Dame, Indiana, (1963).
10. Schubauer, G.B.; and Skramstad, H.K.: Laminar-Boundary-Layer Oscillations and Transition on a Flat Plate. NACA Report No. 909, (1948).
11. Klebanoff, P.S.; Tidstrom, D.K.; and Sargent, L.M.: Boundary Layer Stabilization by Distributed Damping. J. Fluid Mech. Vol. 12, p.1, (1962)
12. Gaster, M.: A Note on the Relation Between Temporally Increasing and Spatially Increasing Disturbances in Hydrodynamic Stability. J. Fluid Mech., Vol. 14, p.222, (1962).
13. Betchov, R., and Criminale, W.O., Jr.: Spatial Stability of the Inviscid Jet and Wake. The Phys. of Fluid, Vol. 9, No. 2, p.359, (1966).

14. Smith, A.M.O.: Improved Solutions of the Falkner and Skan Boundary-Layer Equation. Inst. of the Aero. Sci., S.M.F. paper No. FF-10, (1954).

15. Tollmien, W.: A General Criterion of the Instability of Laminar Velocity Distributions. Nachricht. d. Ges. D. Wiss. Göttingsen, Math. Phys. Klasse, (1935) p.79.

16. Radbill, J.R., et al: A New Method for Prediction of Stability of Laminar Boundary Layers. Report No. C6-1019/020 of North American Aviation, Inc., Anaheim, Calif., also available as AFOSR-66-0702 or AD 633-978 (1966).

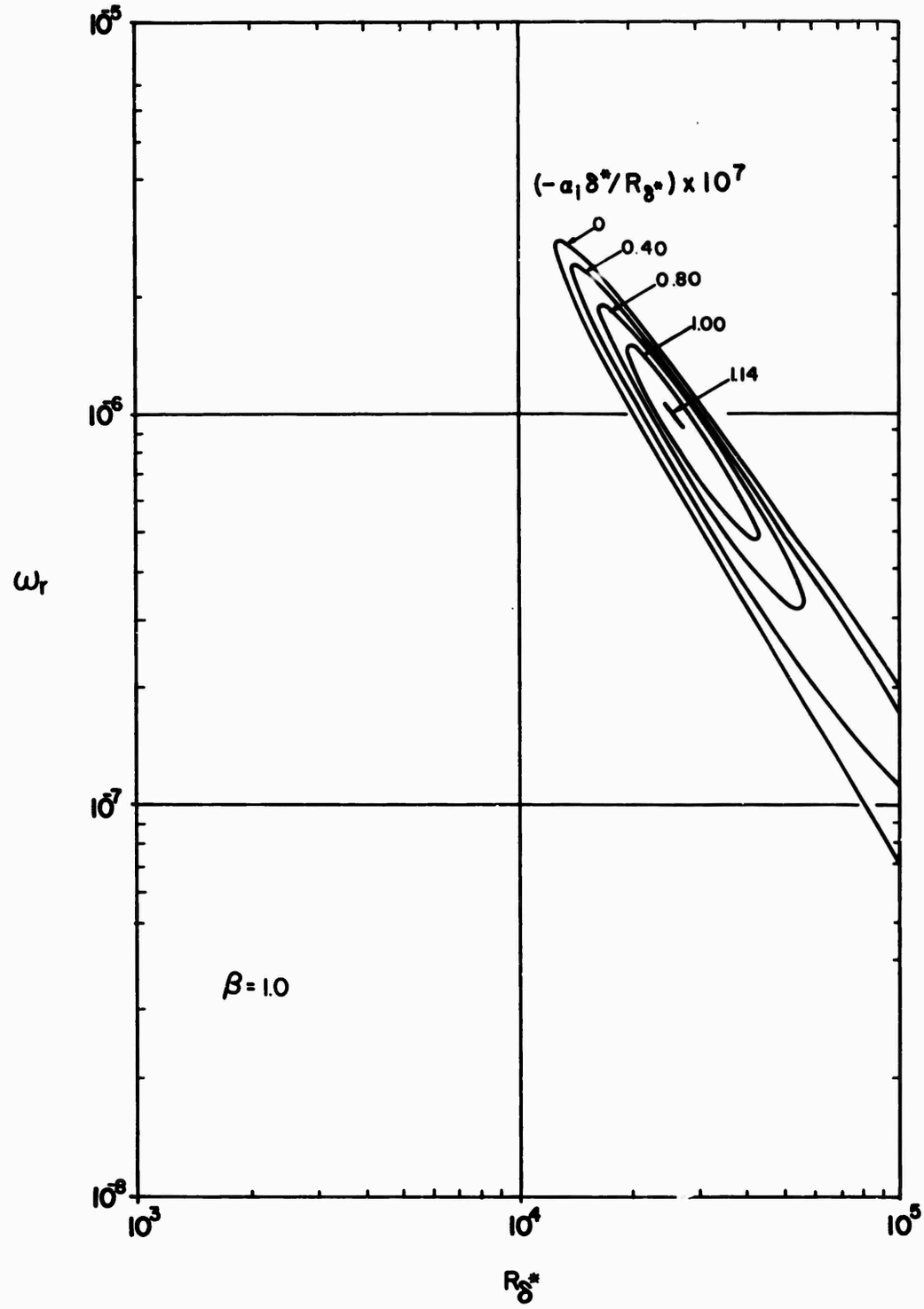

Figure 1. - Curves of constant spatial amplification rates ($\beta = 1.0$)

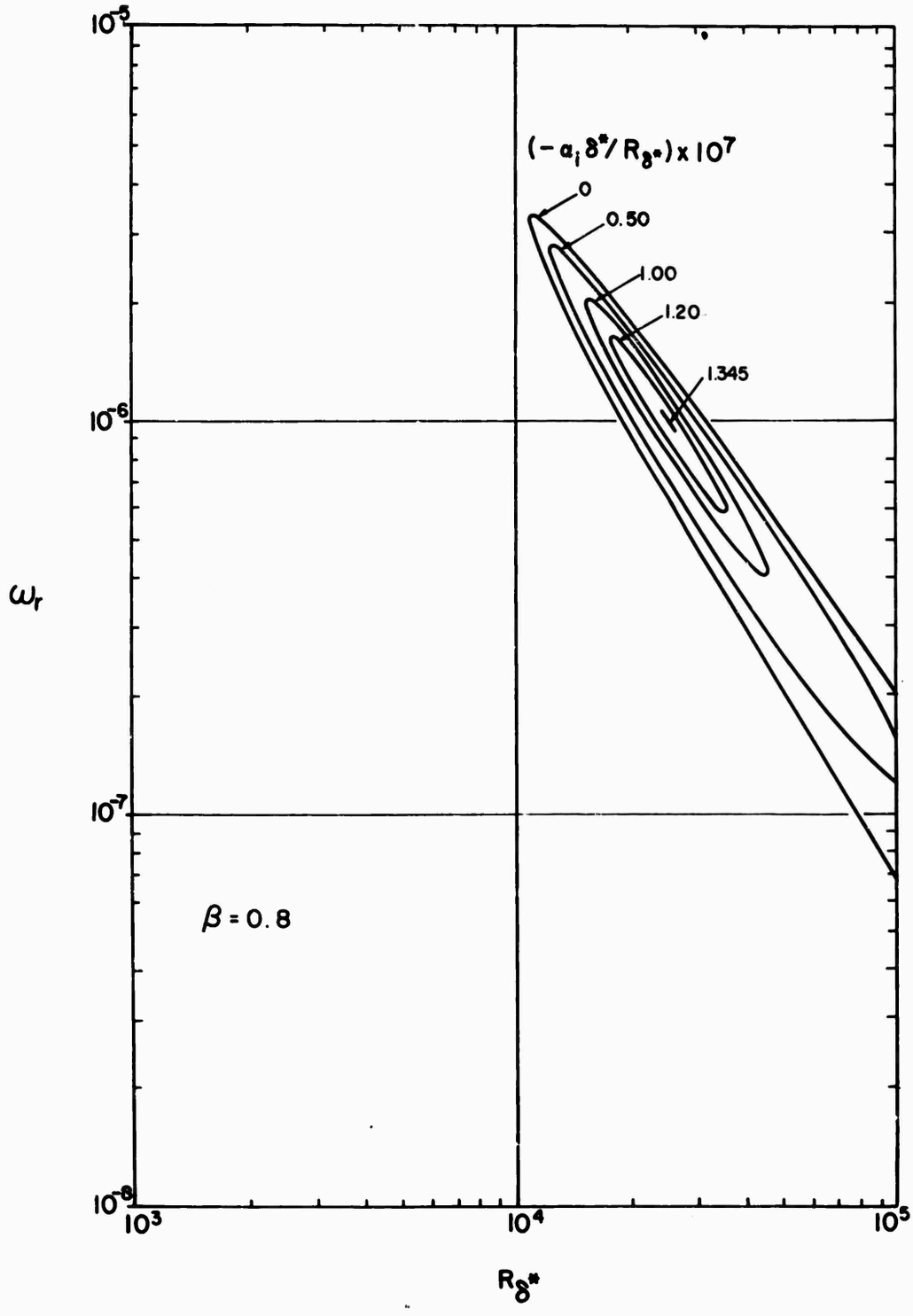

Figure 2. - Curves of constant spatial amplification rates ($\beta = 0.8$)

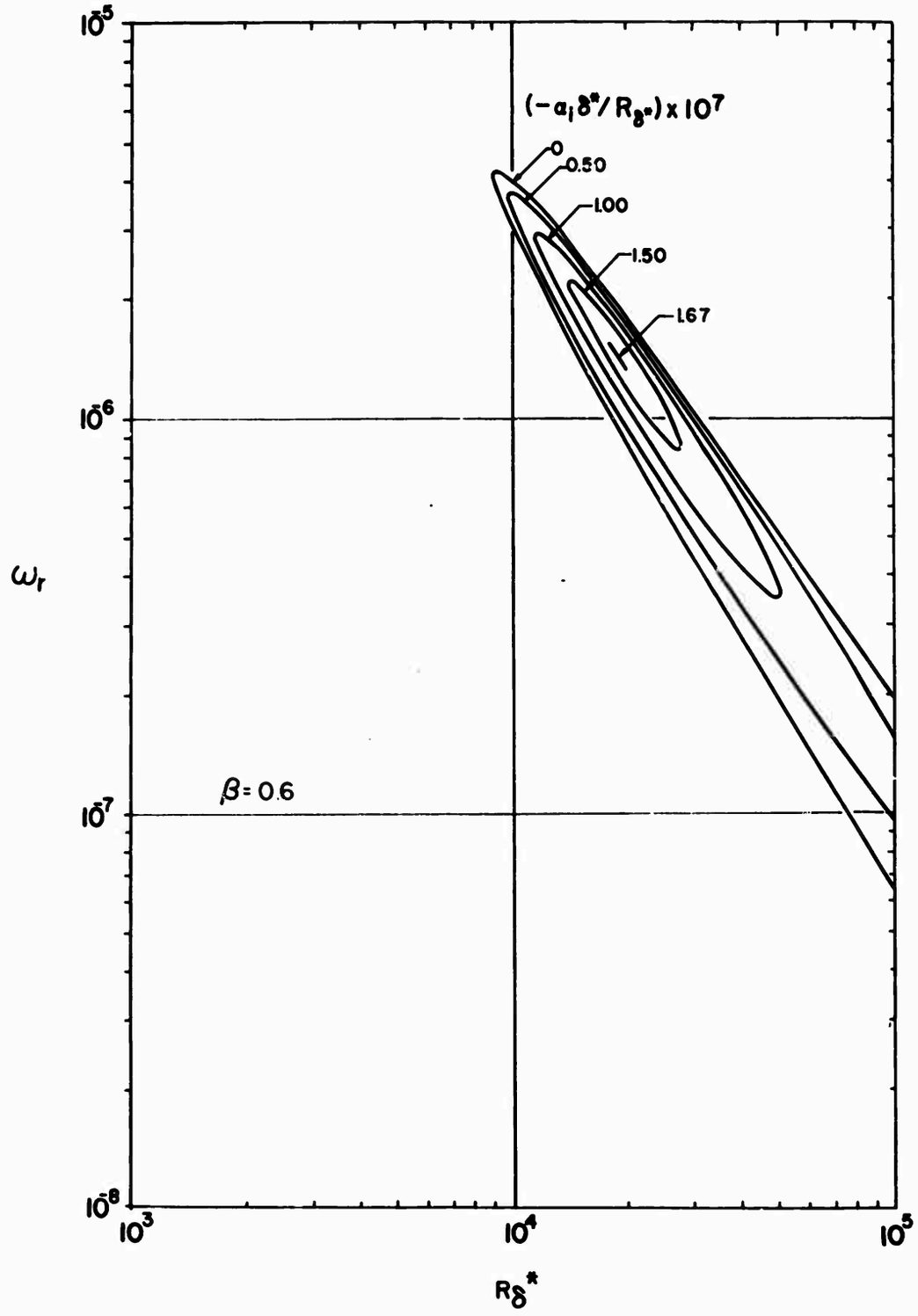

Figure 3. - Curves of constant spatial amplification rates ($\beta = 0.6$)

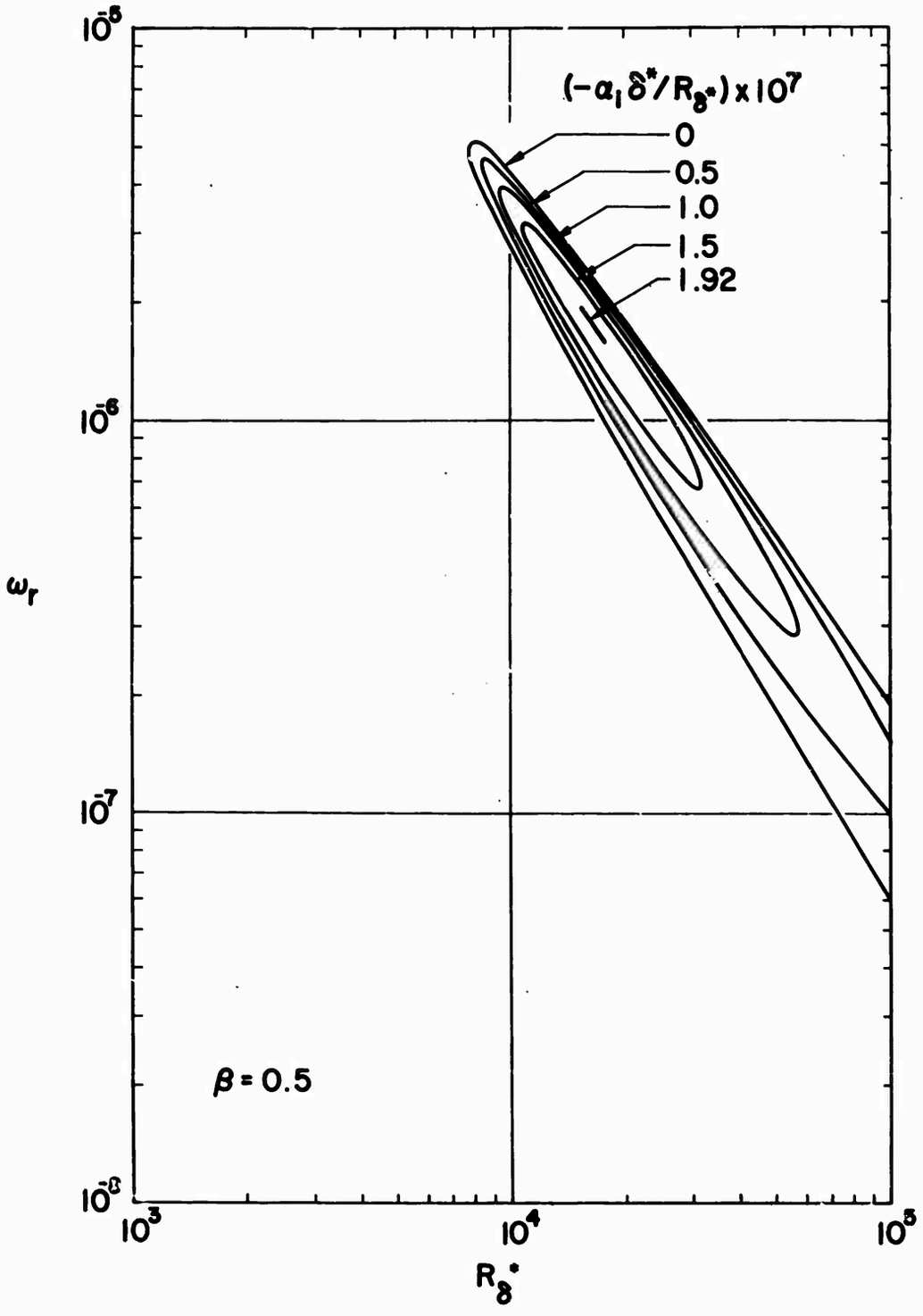

Figure 4. - Curves of constant spatial amplification rates ($\beta = 0.5$)

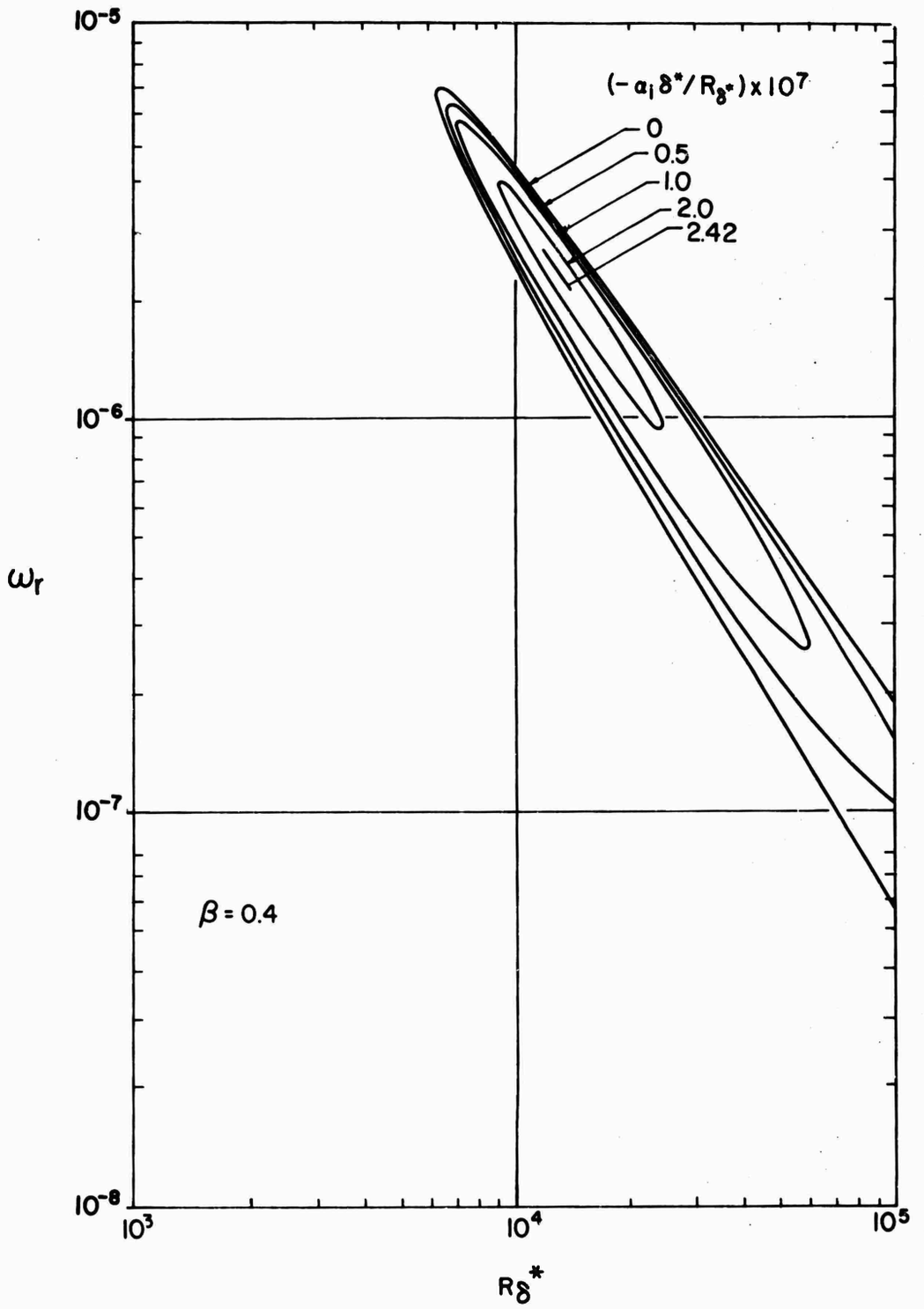

Figure 5. - Curves of constant spatial amplification rates ($\beta = 0.4$)

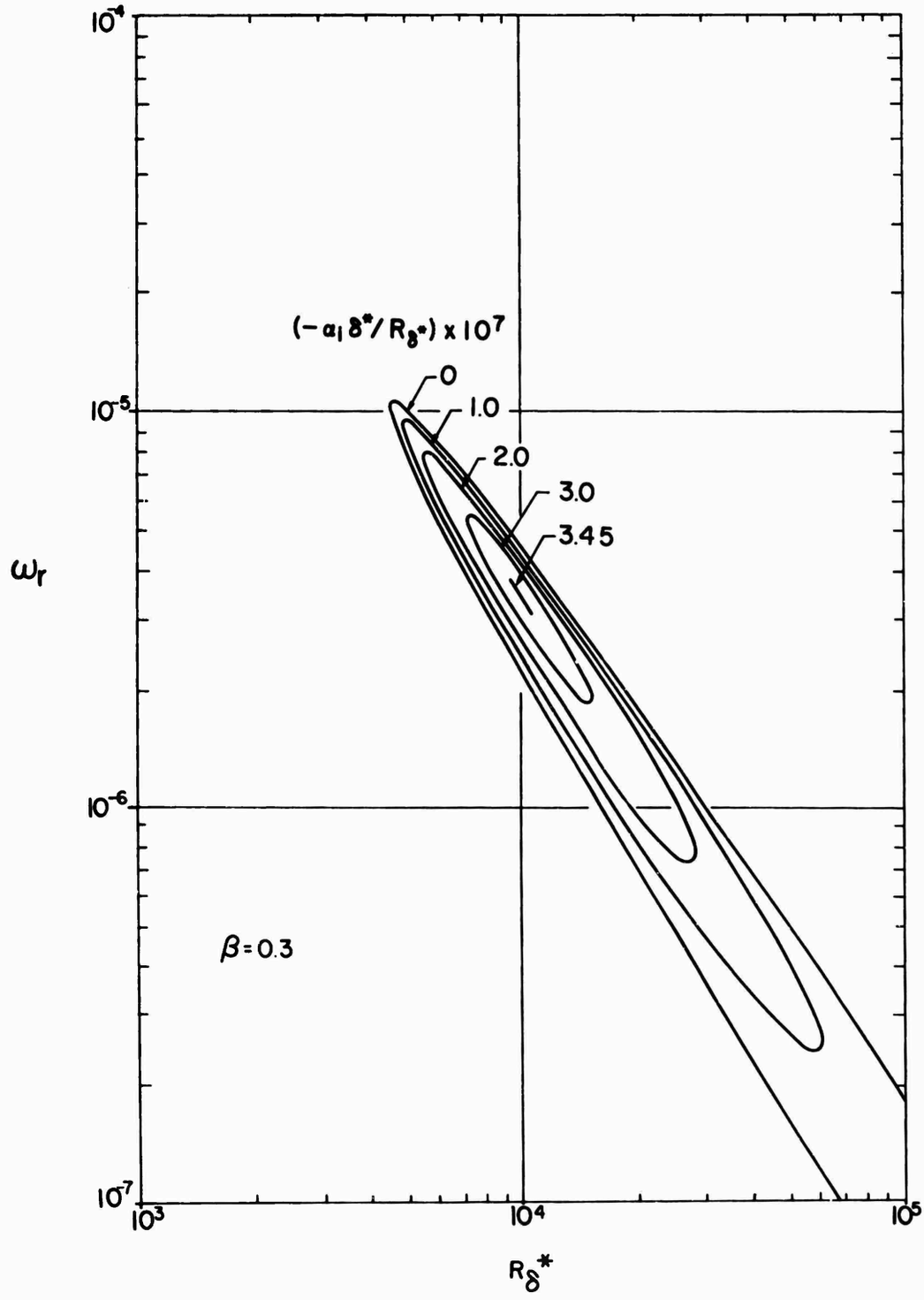

Figure 6. - Curves of constant spatial amplification rates ($\beta = 0.3$)

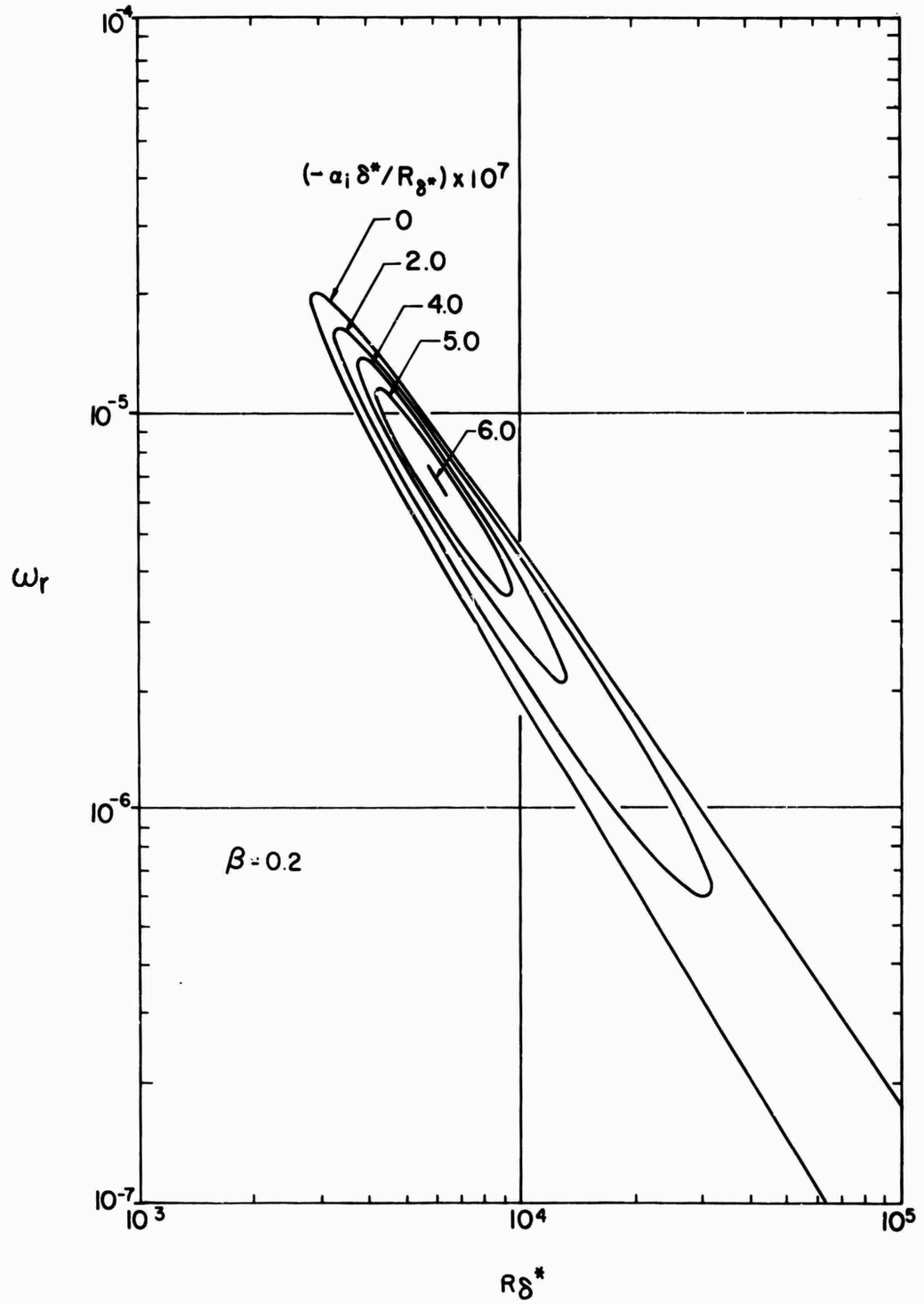

Figure 7. - Curves of constant spatial amplification rates ($\beta = 0.2$)

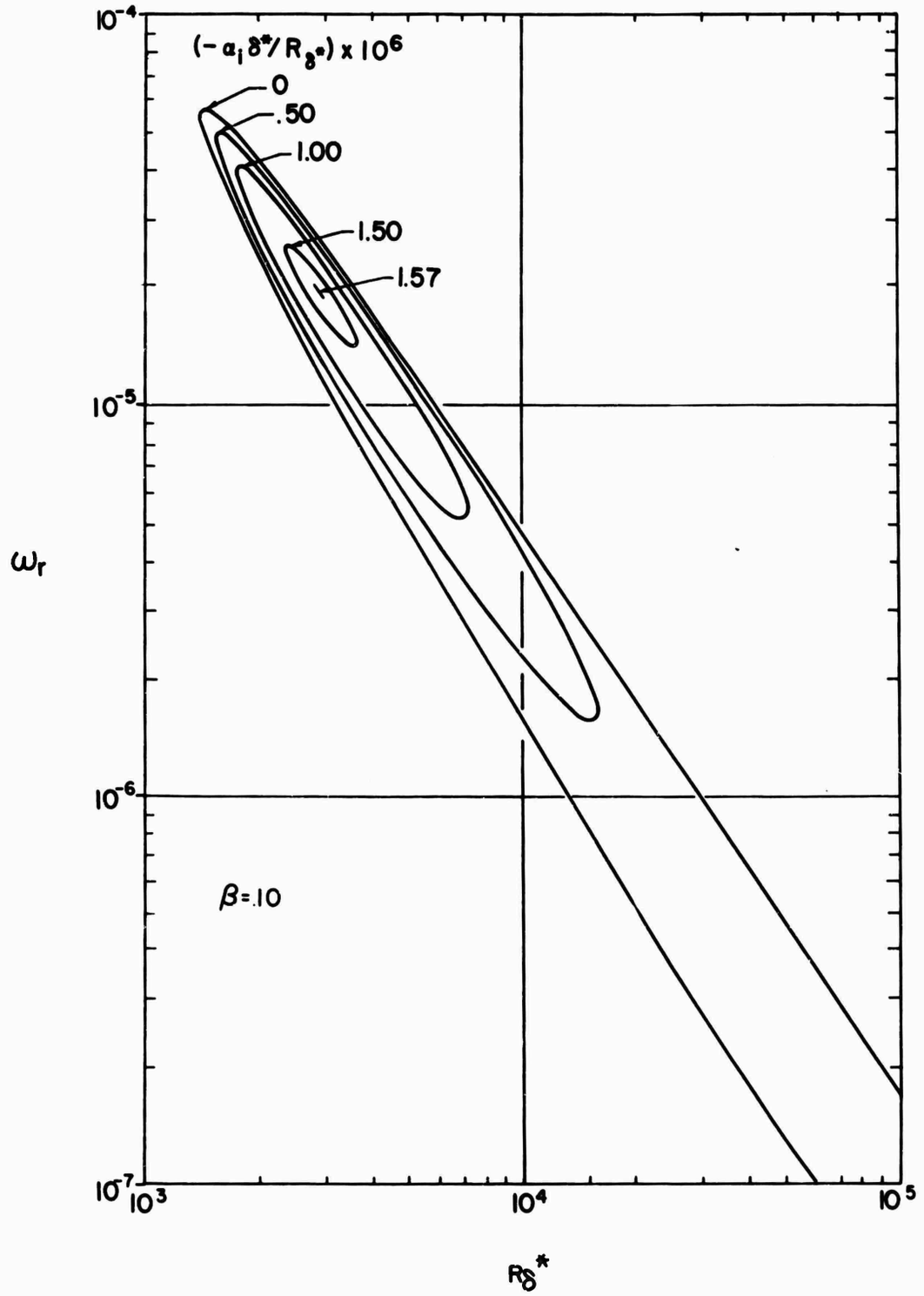

Figure 8. - Curves of constant spatial amplification rates ($\beta = 0.1$)

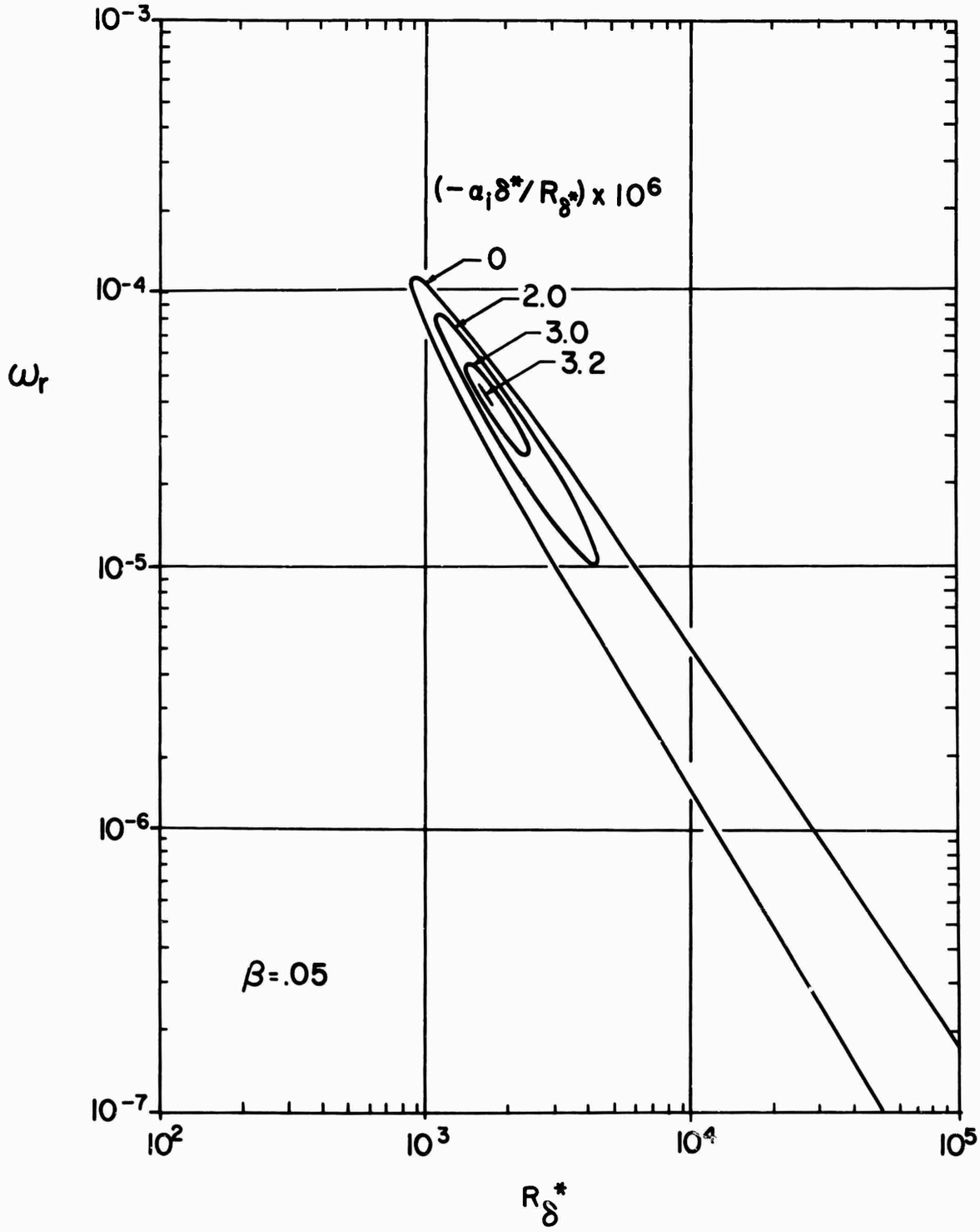

Figure 9. - Curves of constant spatial amplification rates ($\beta = 0.05$)

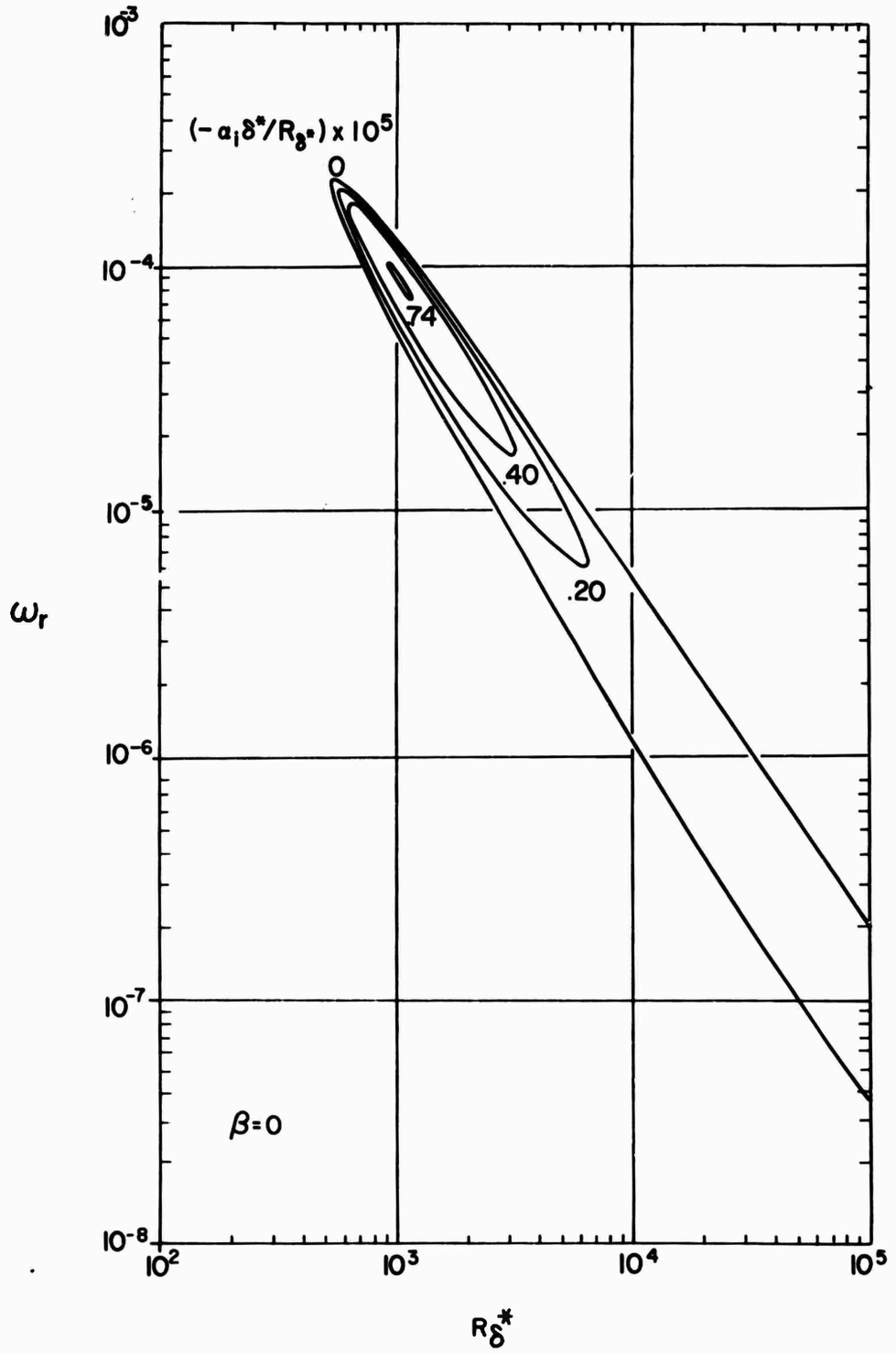

Figure 10. - Curves of constant spatial amplification rates ($\beta = 0$)

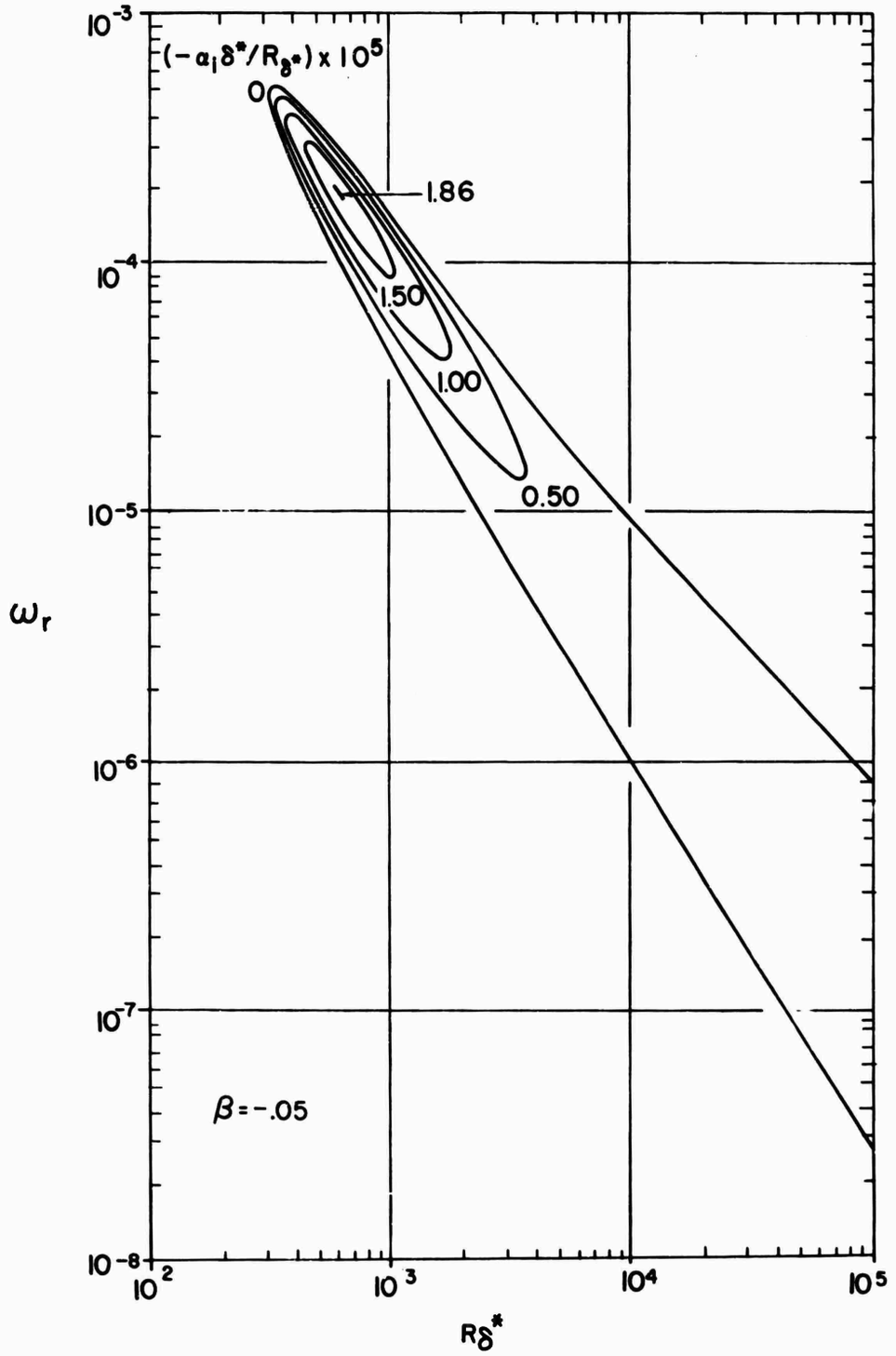

Figure 11. - Curves of constant spatial amplification rates ($\beta = -0.05$)

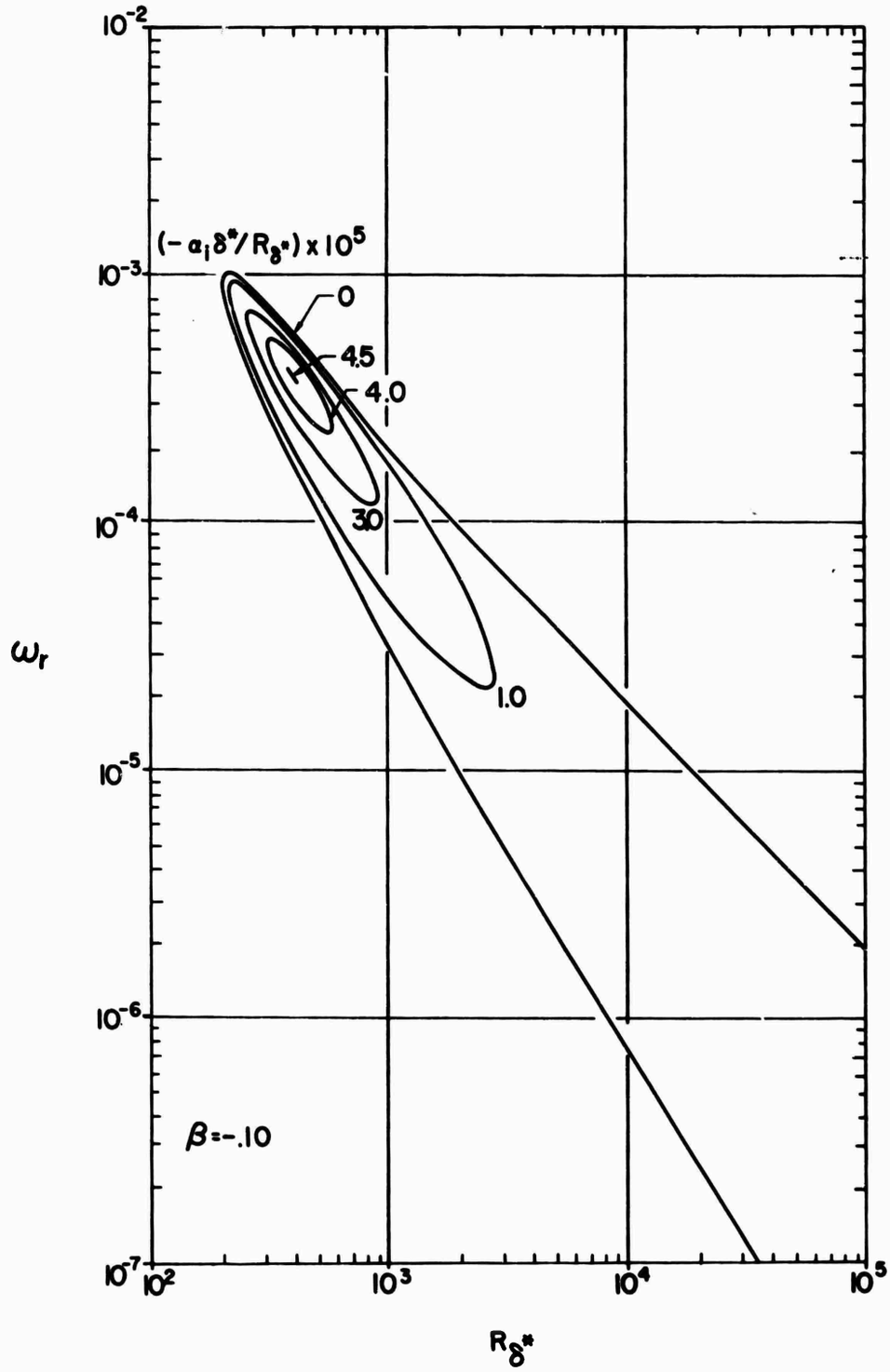

Figure 12. - Curves of constant spatial amplification rates ($\beta = -0.10$)

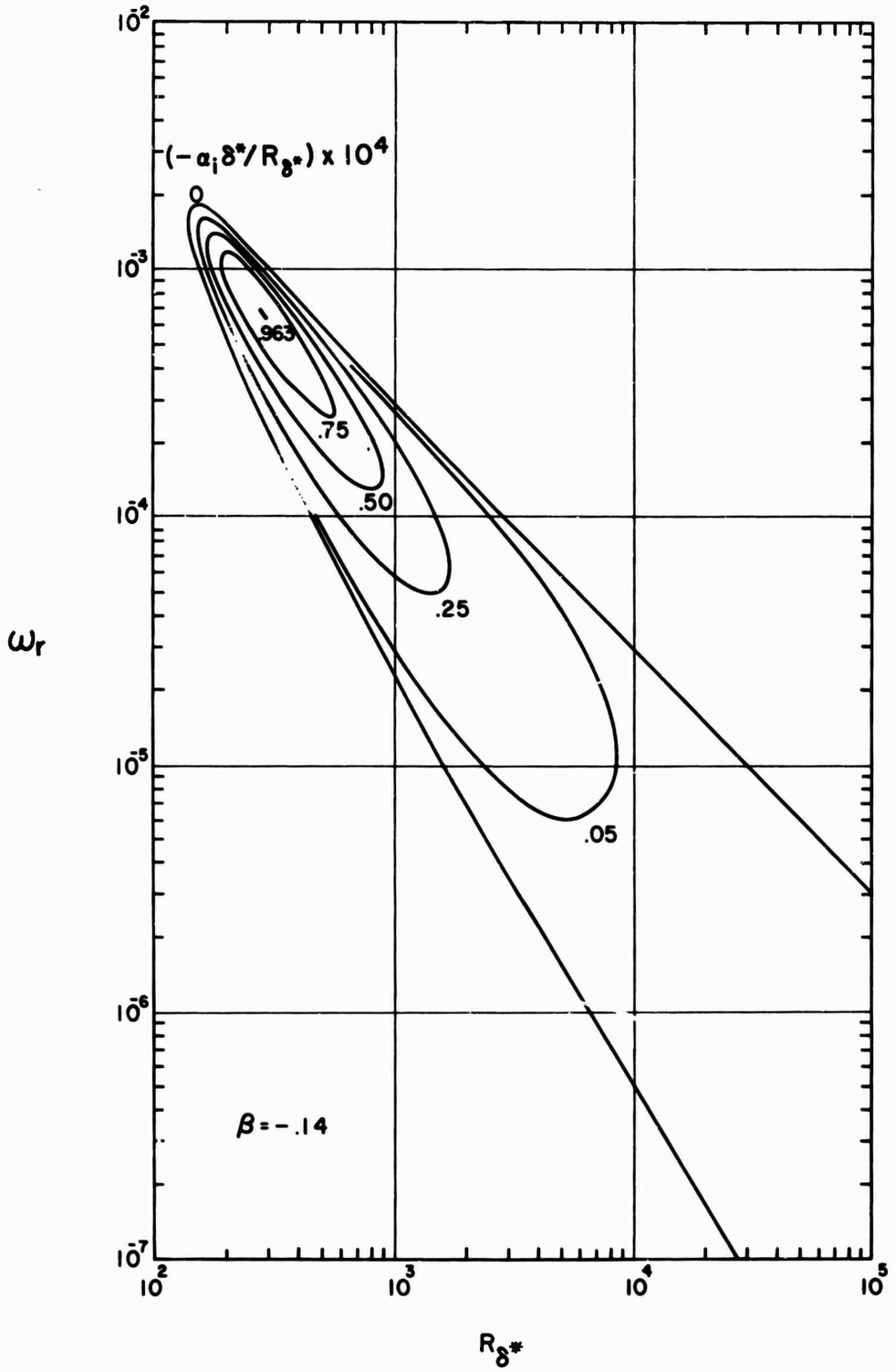

Figure 13. - Curves of constant spatial amplification rates ($\beta = -0.14$)

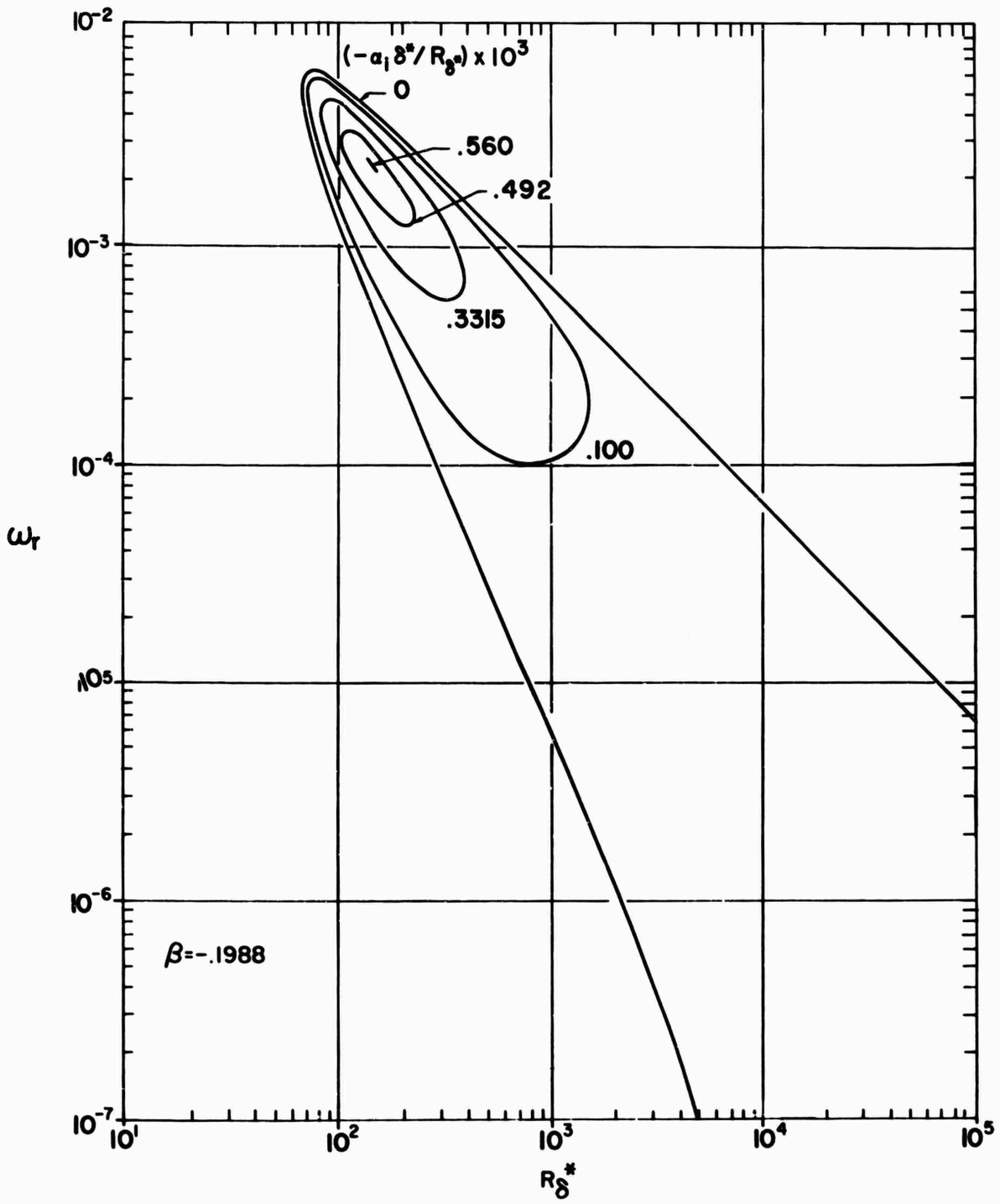

Figure 14. - Curves of constant spatial amplification rates (β = –0.1988)

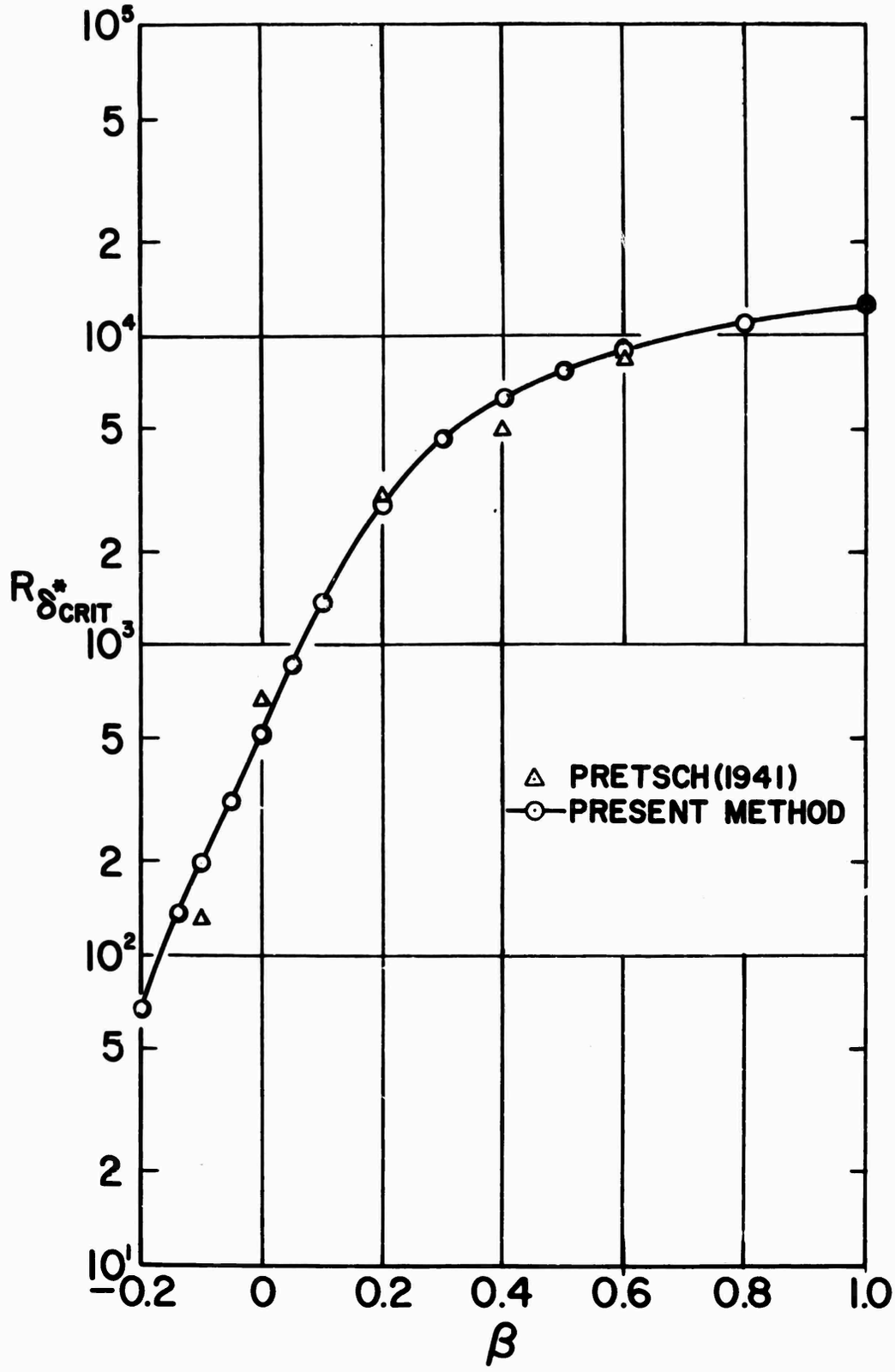

Figure 15.—Effect of pressure gradient on the critical Reynolds number

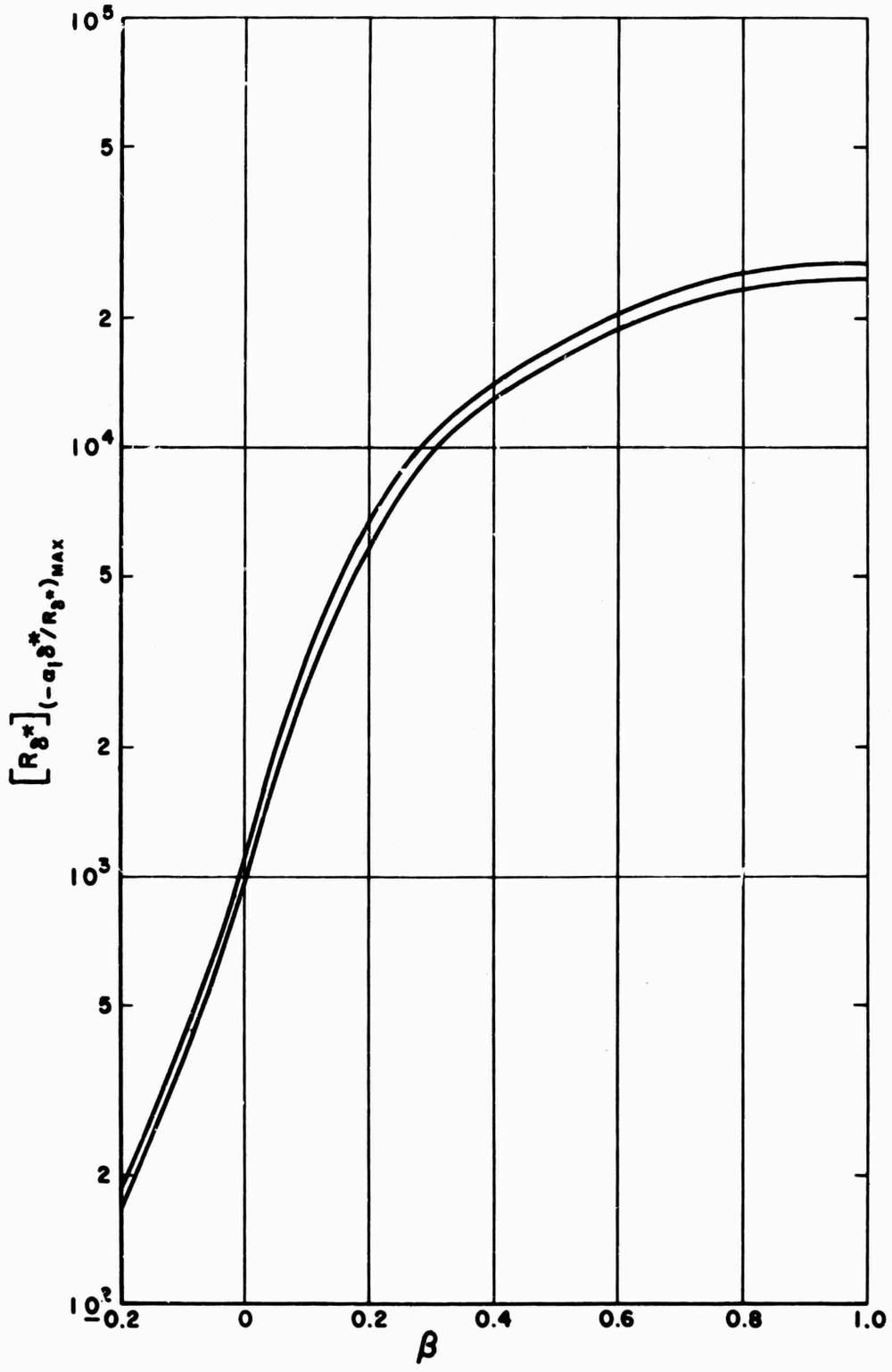

Figure 16. - Upper and lower bounds of the Reynolds number at maximum spatial amplification rate.

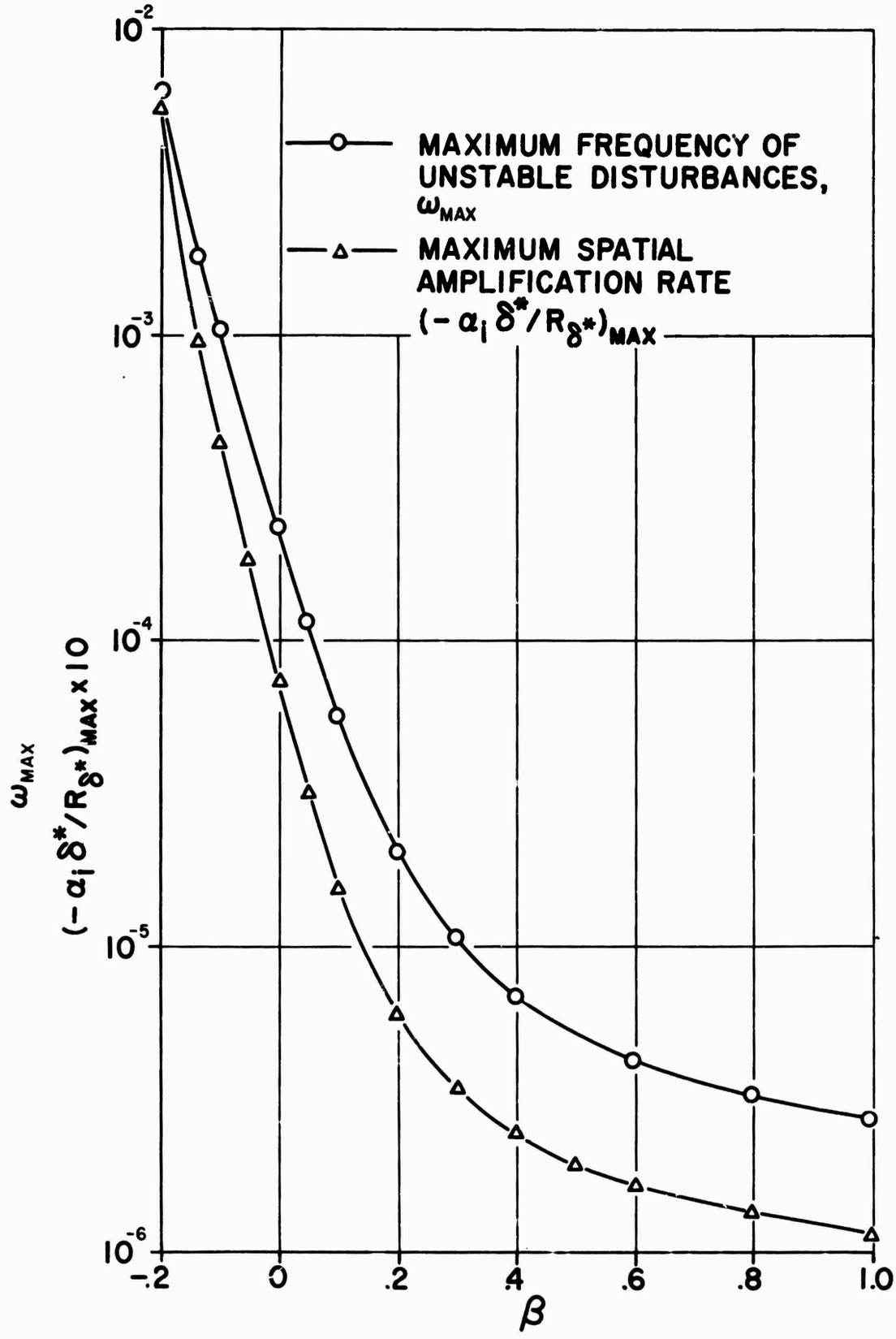

Figure 17. - Effect of pressure gradient on the maximum spatial amplification rate and frequency of unstable disturbances

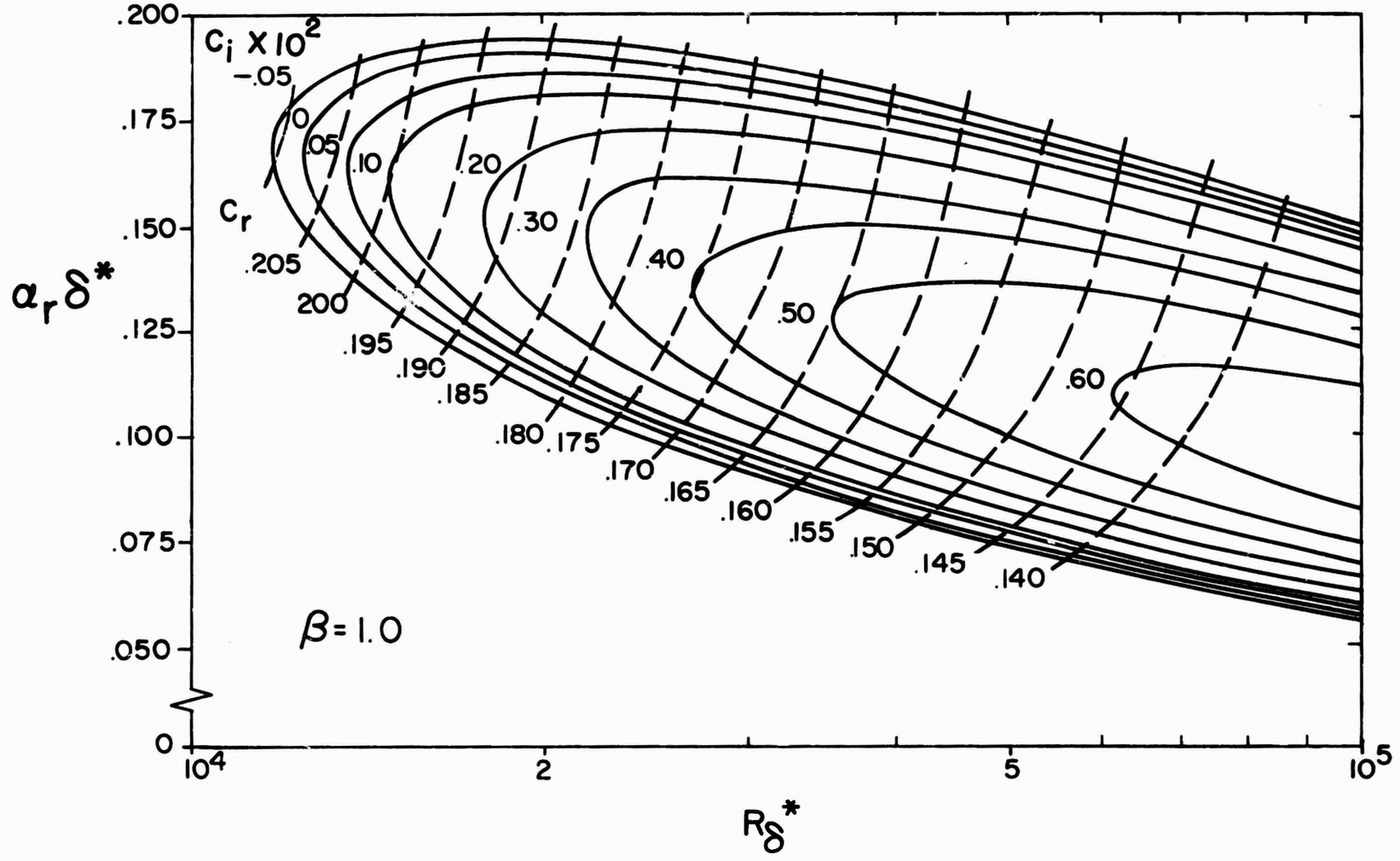

Figure 18. - Curves of constant temporal amplification rates (β = 1.0)

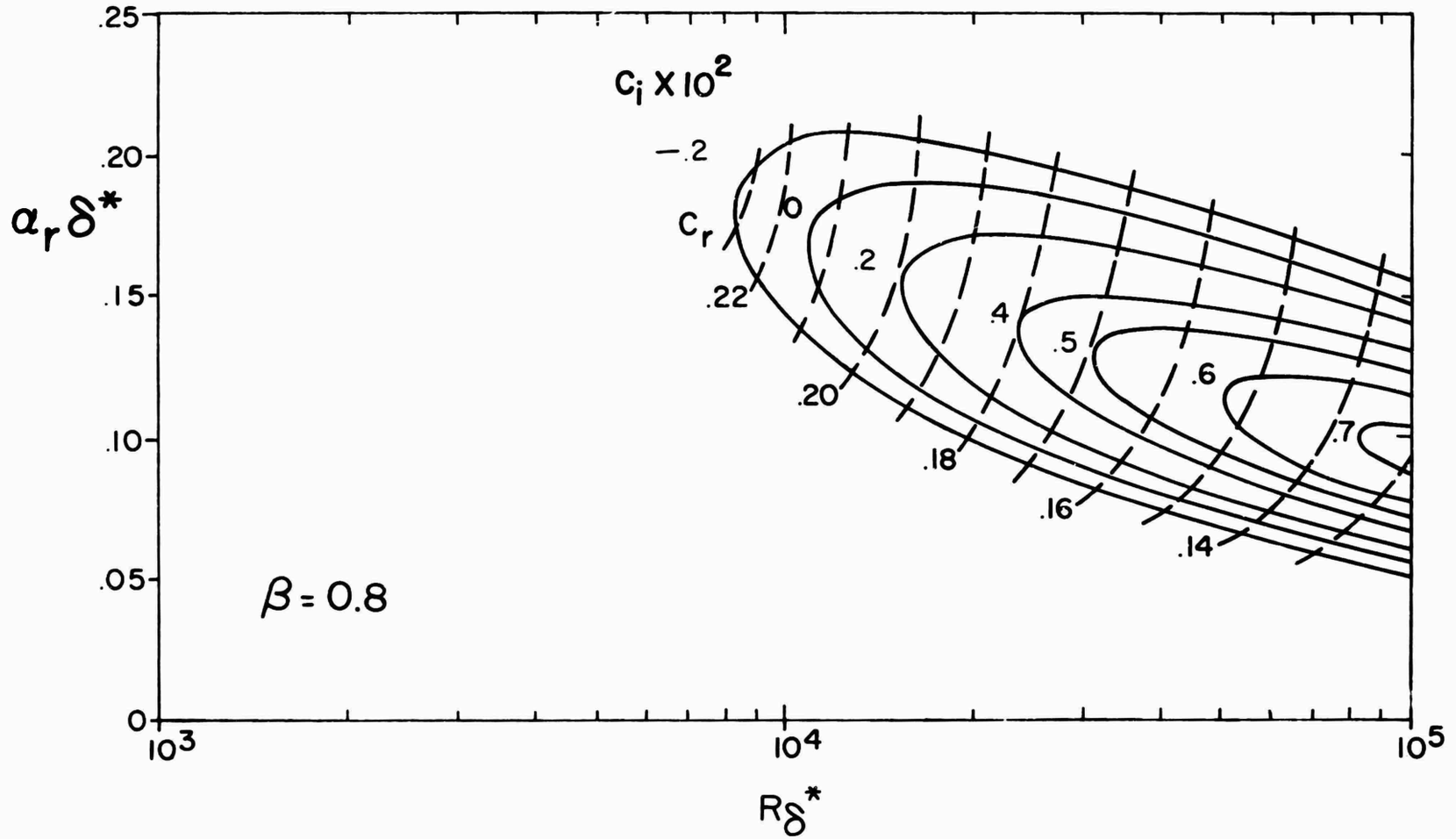

Figure 19. - Curves of constant temporal amplification rates ($\beta = 0.8$)

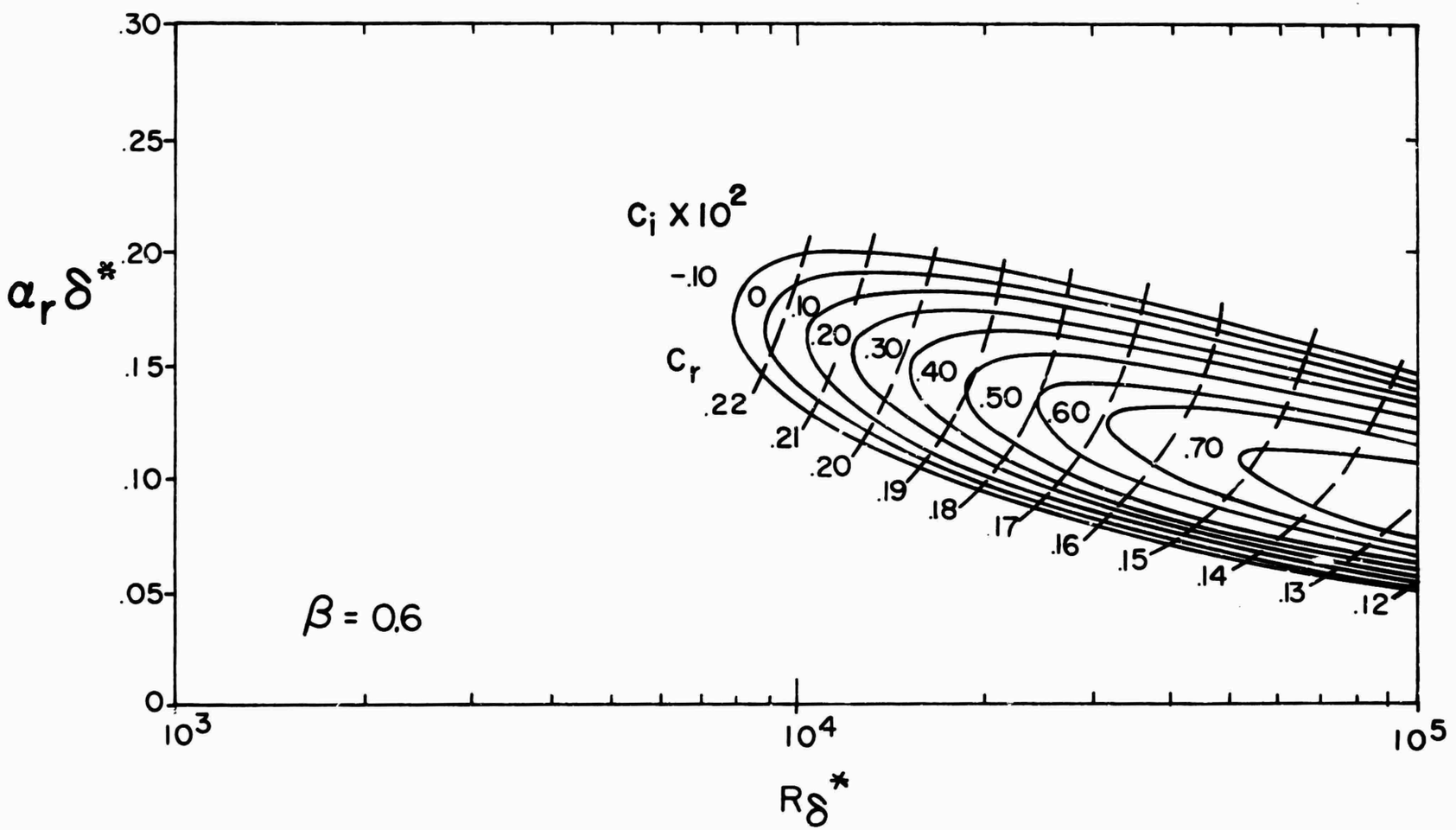

Figure 20. - Curves of constant temporal amplification rates ($\beta = 0.6$)

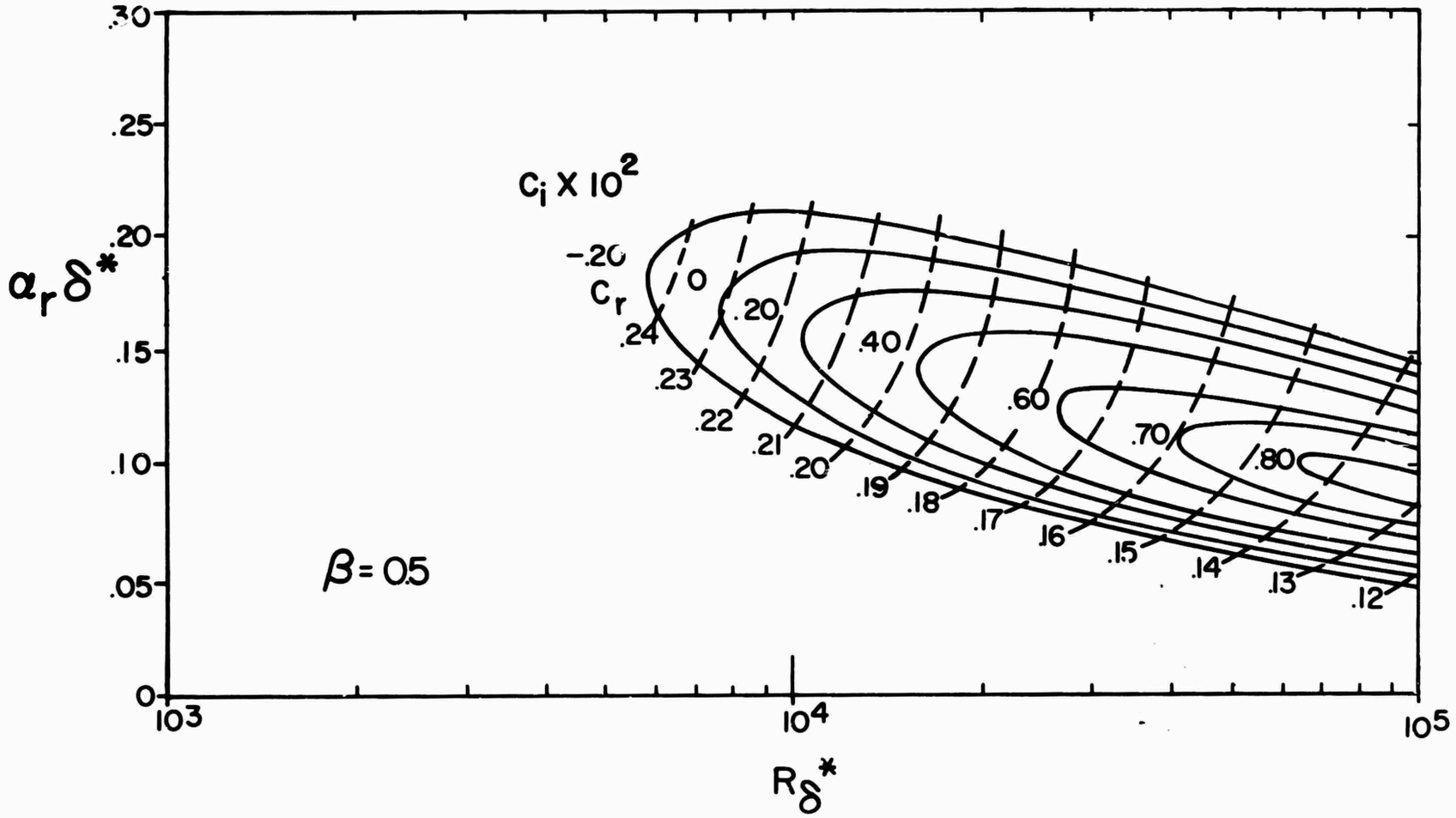

Figure 21. - Curves of constant temporal amplification rates ($\beta = 0.5$)

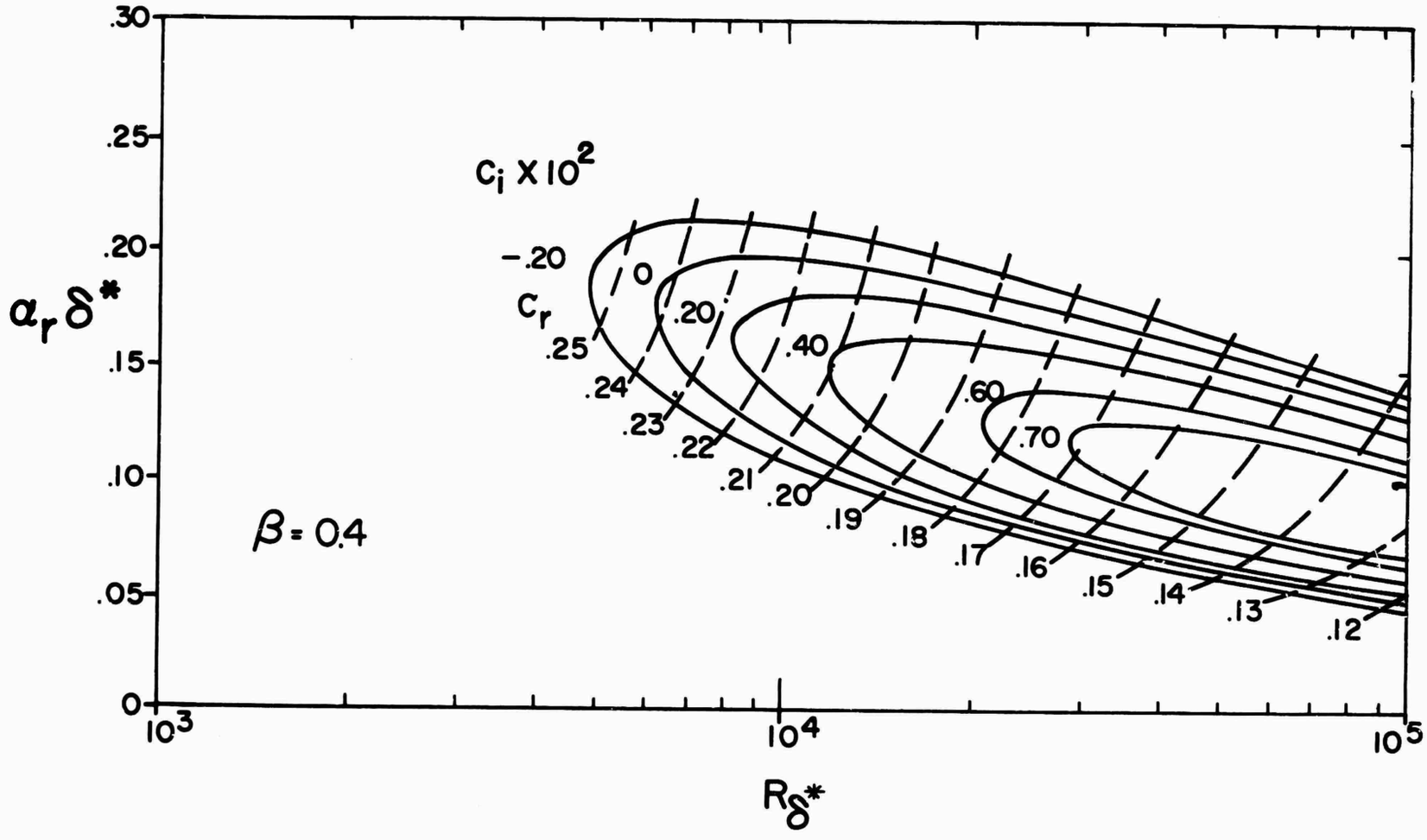

Figure 22. - Curves of constant temporal amplification rates ($\beta = 0.4$)

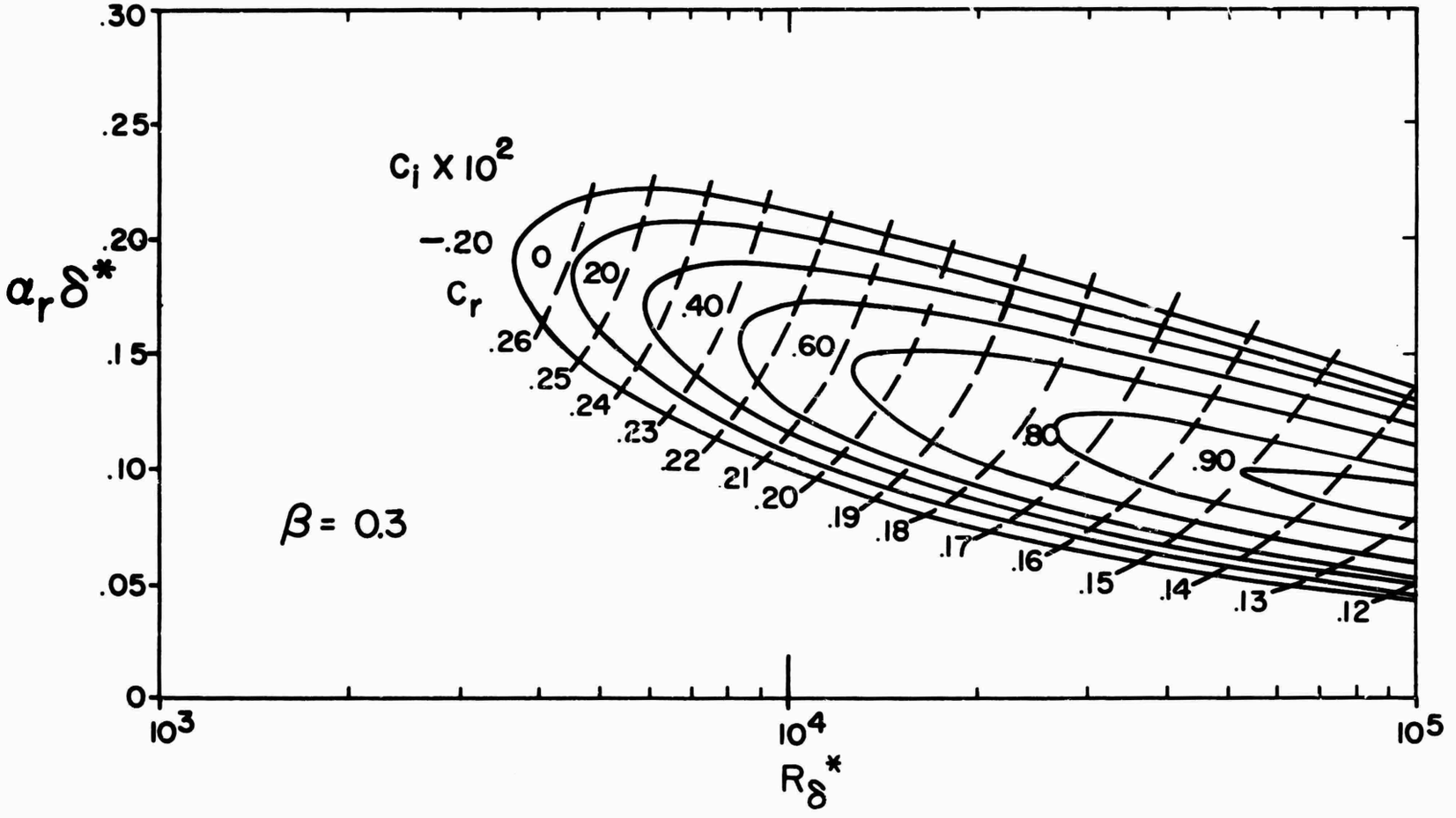

Figure 23. - Curves of constant temporal amplification rates ($\beta = 0.3$)

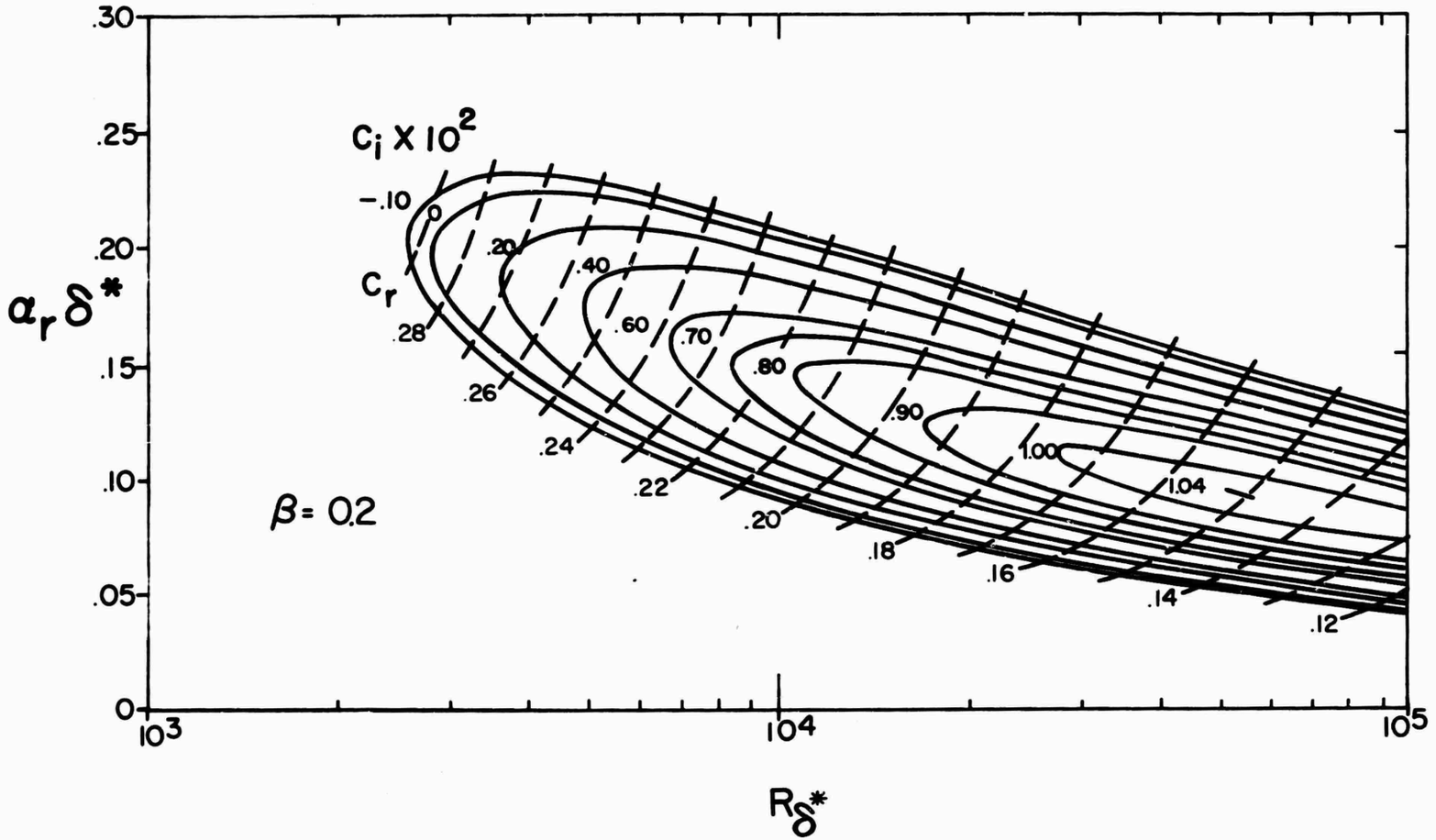

Figure 24. - Curves of constant temporal amplification rates ($\beta = 0.2$)

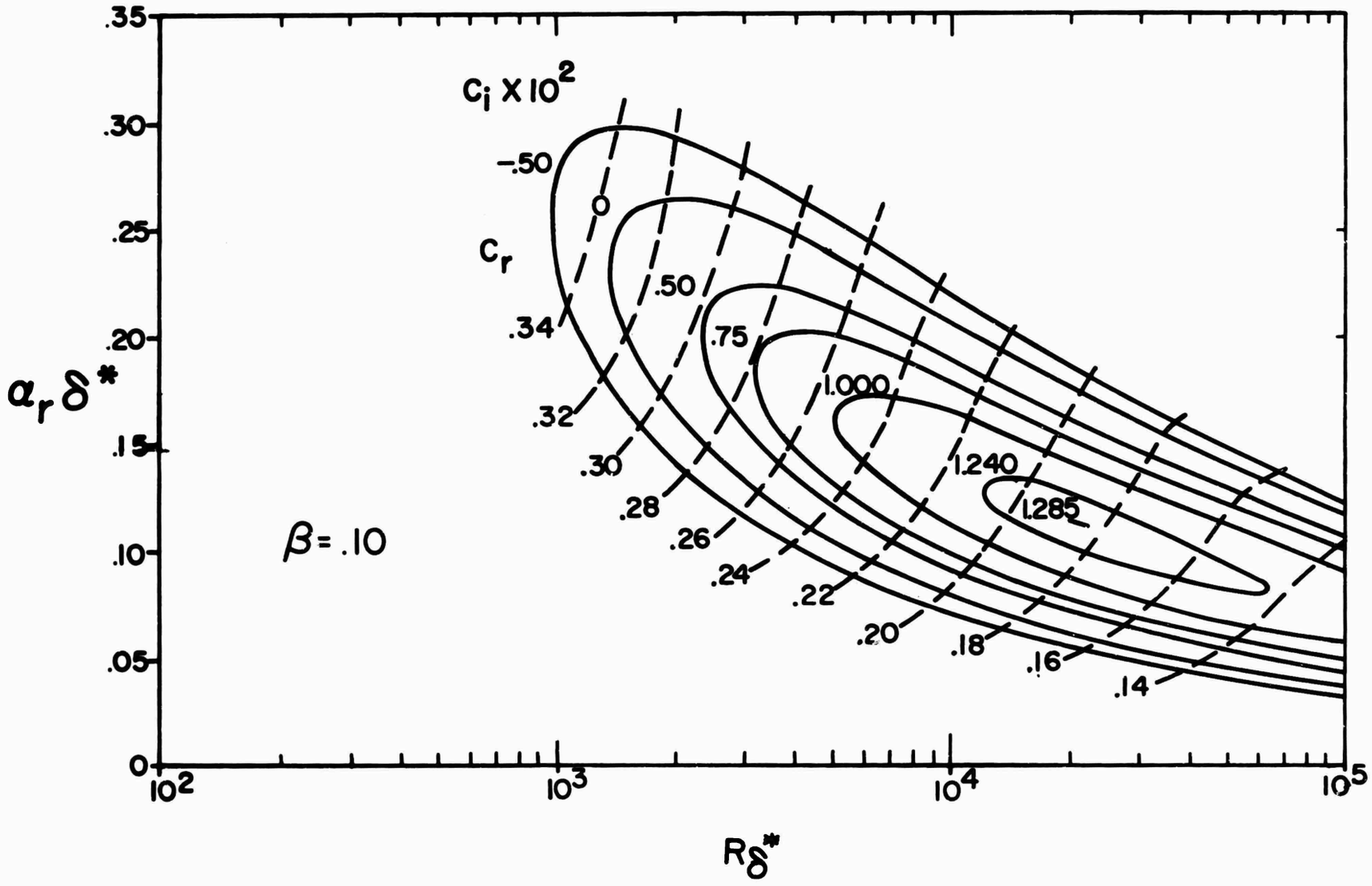

Figure 25. - Curves of constant temporal amplification rates ($\beta = 0.1$)

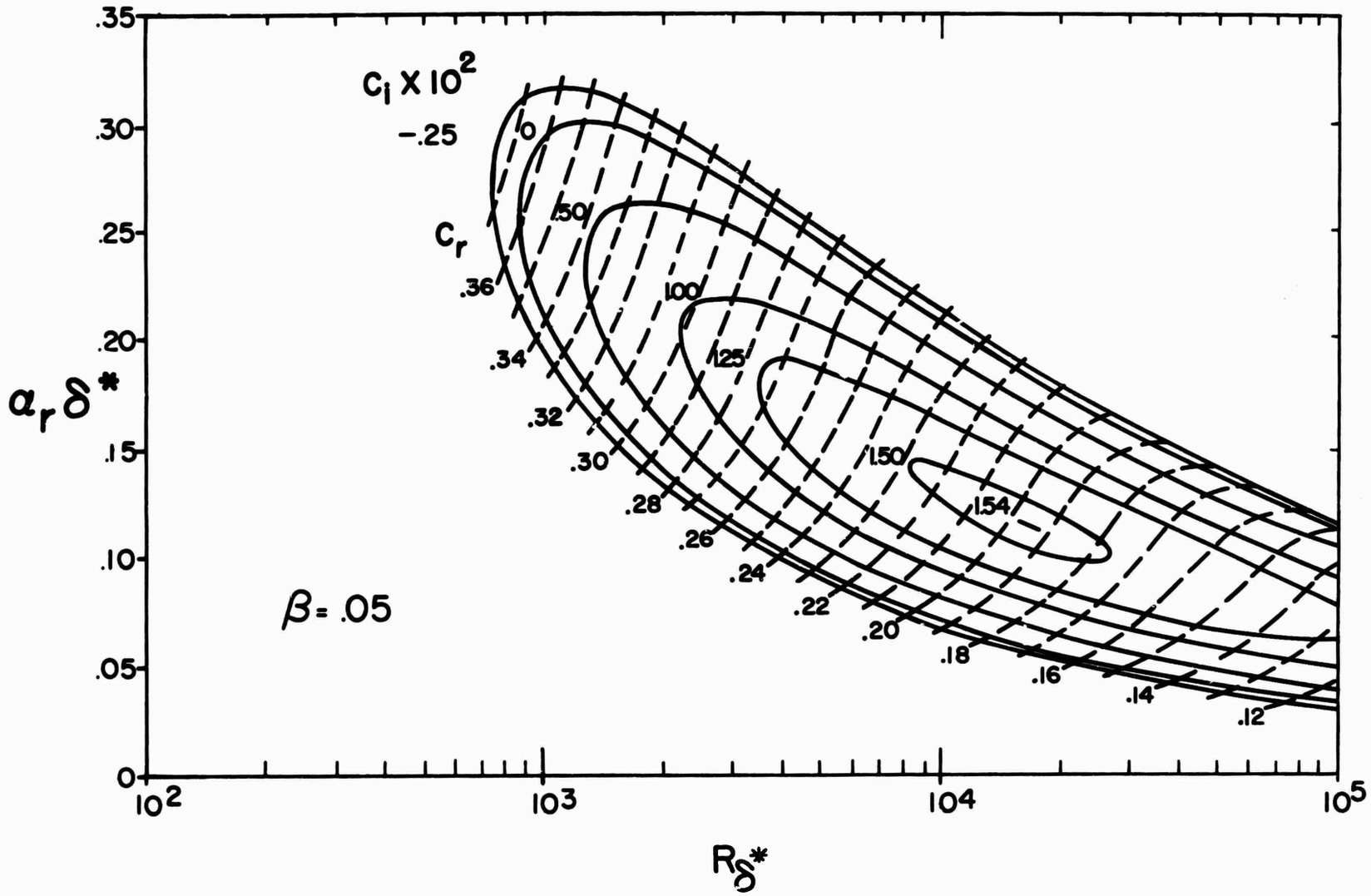

Figure 26. - Curves of constant temporal amplification rates ($\beta = 0.05$)

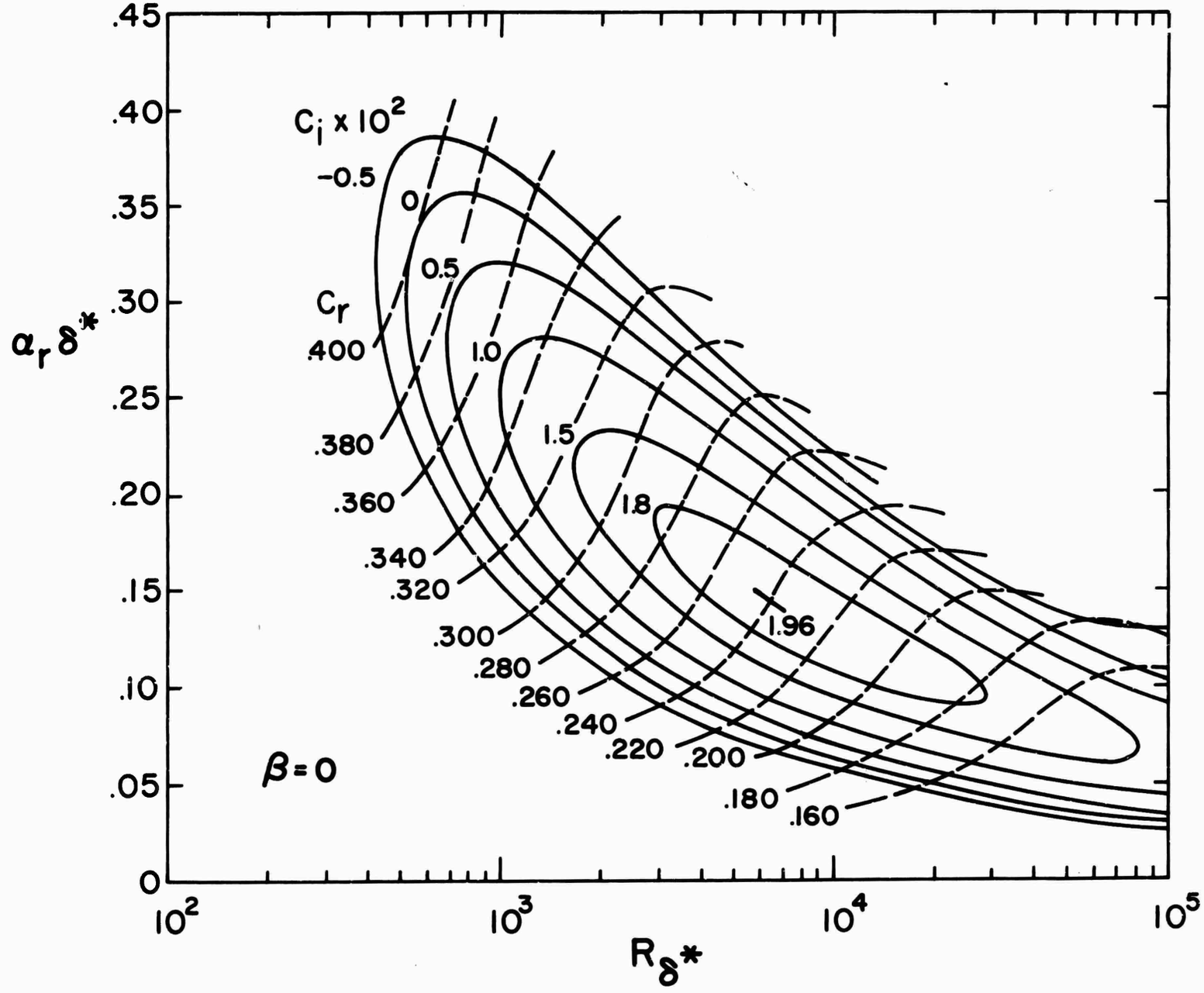

Figure 27. - Curves of constant temporal amplification rates ($\beta = 0$)

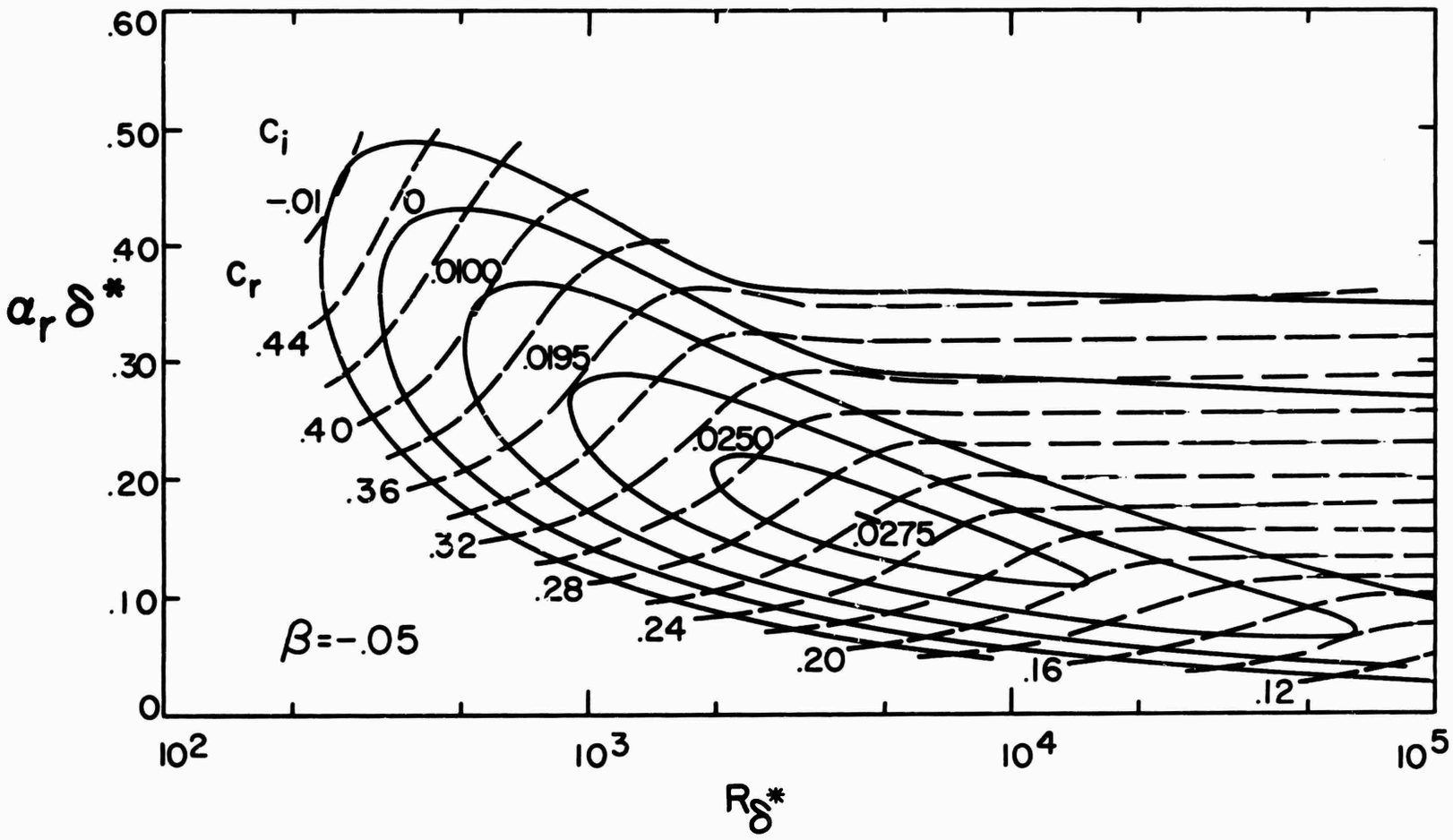

Figure 28. - Curves of constant temporal amplification rates ($\beta = -0.05$)

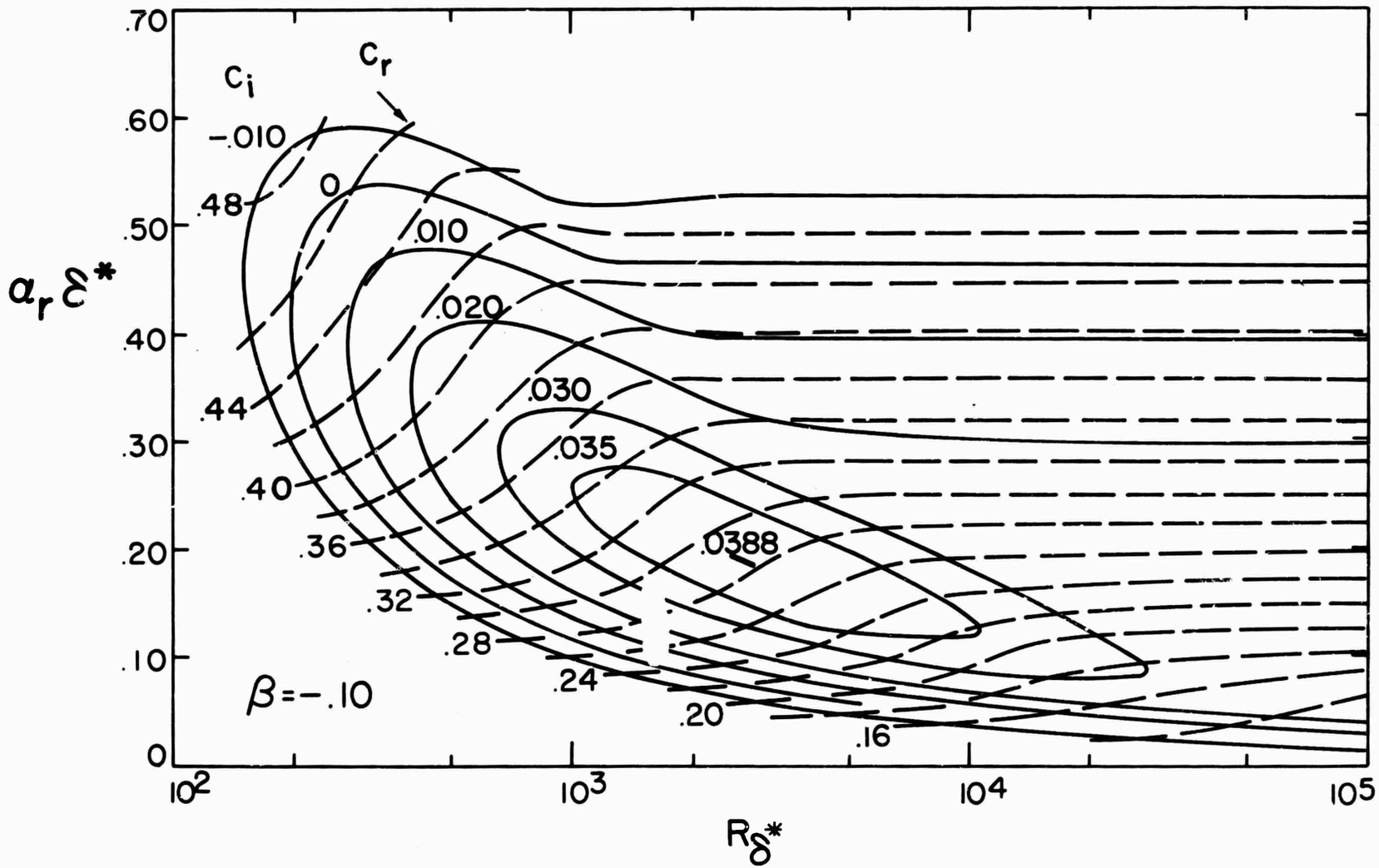

Figure 29. - Curves of constant temporal amplification rates ($\beta = -0.10$)

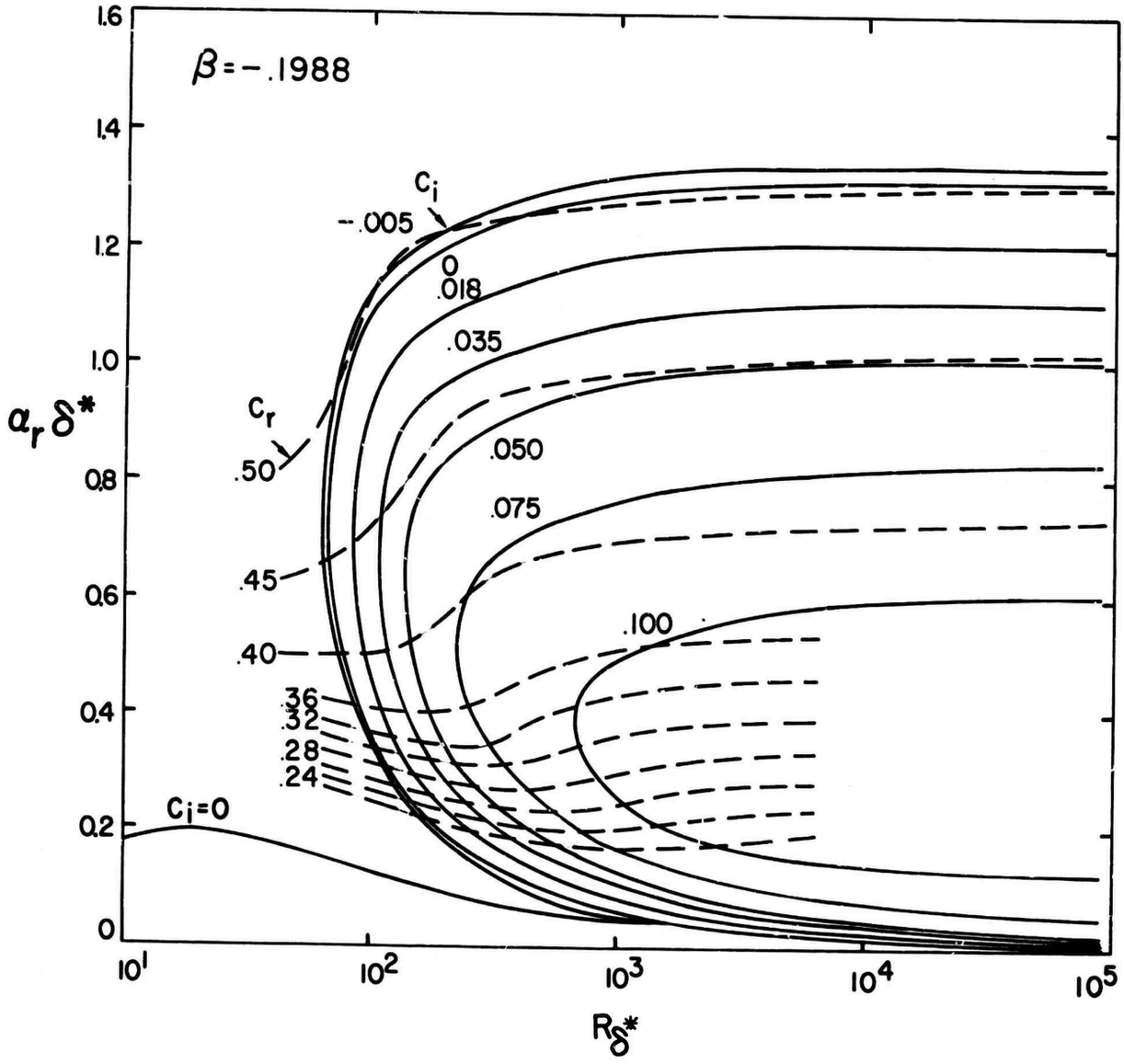

Figure 31. - Curves of constant temporal amplification rates ($\beta = -0.1988$)

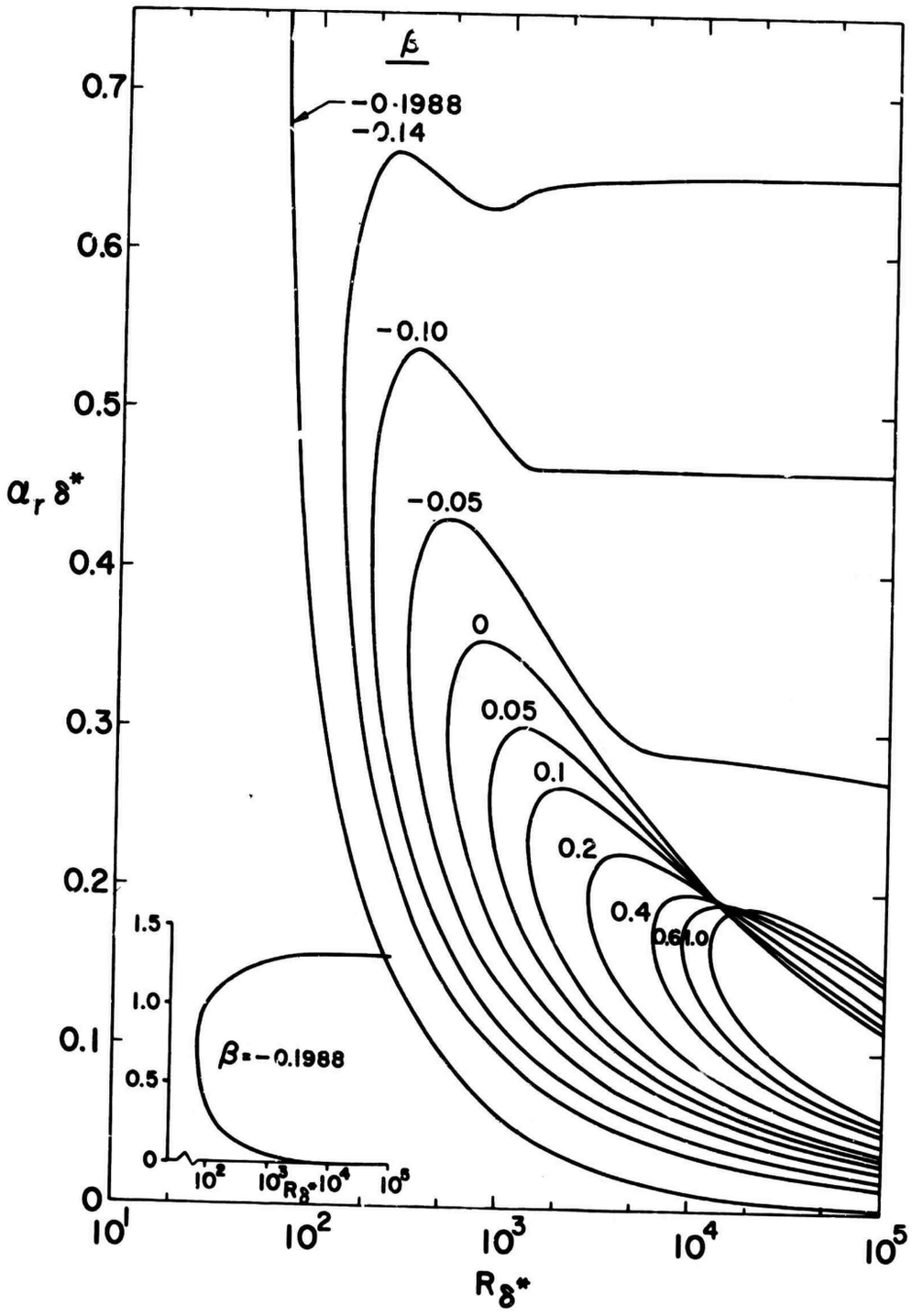

Figure 32. - Curves of neutral stability for the Hartree β boundary-layer profiles

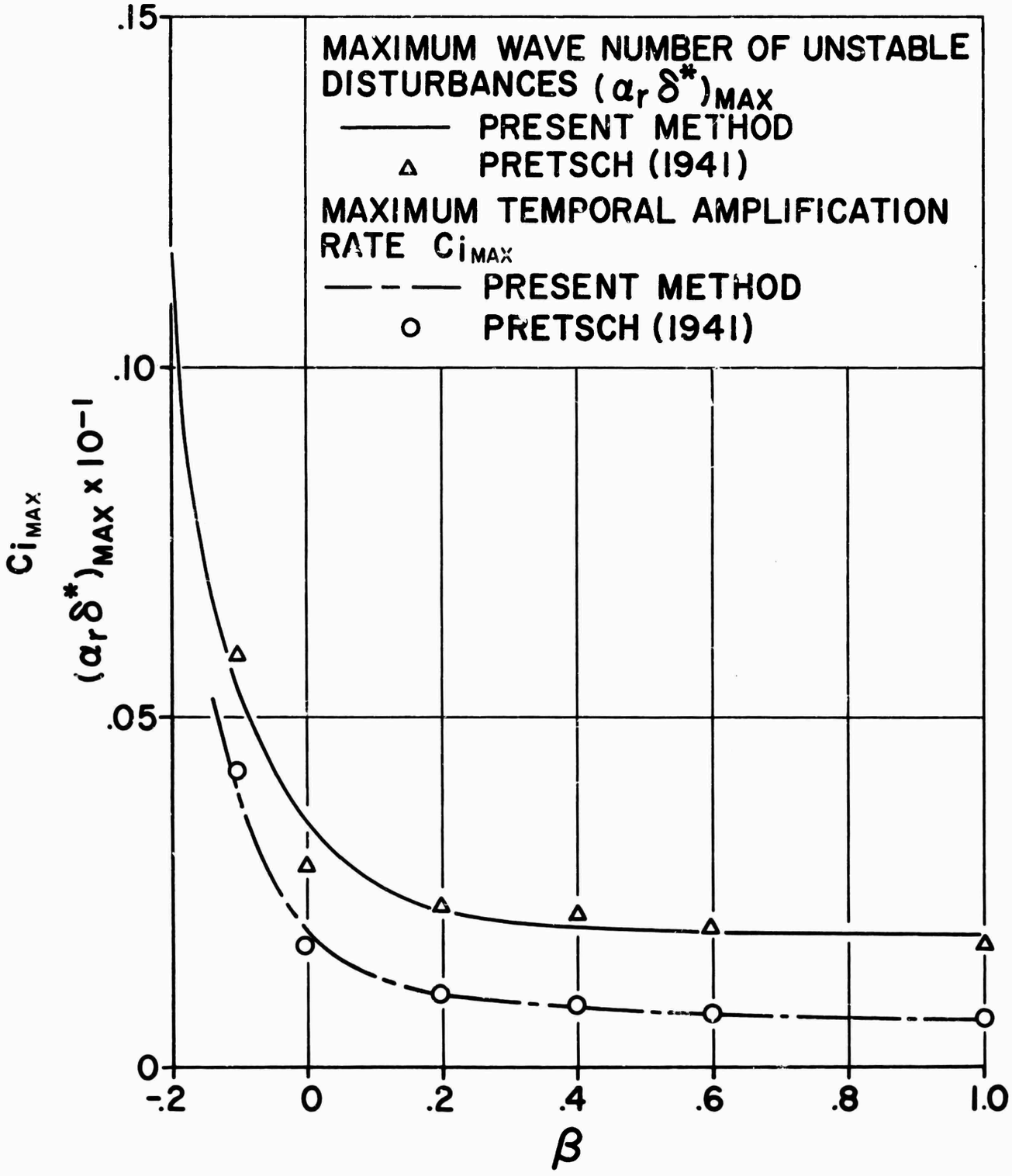

Figure 33. - Effect of pressure gradient on the maximum temporal amplification rate and wave number of unstable disturbances

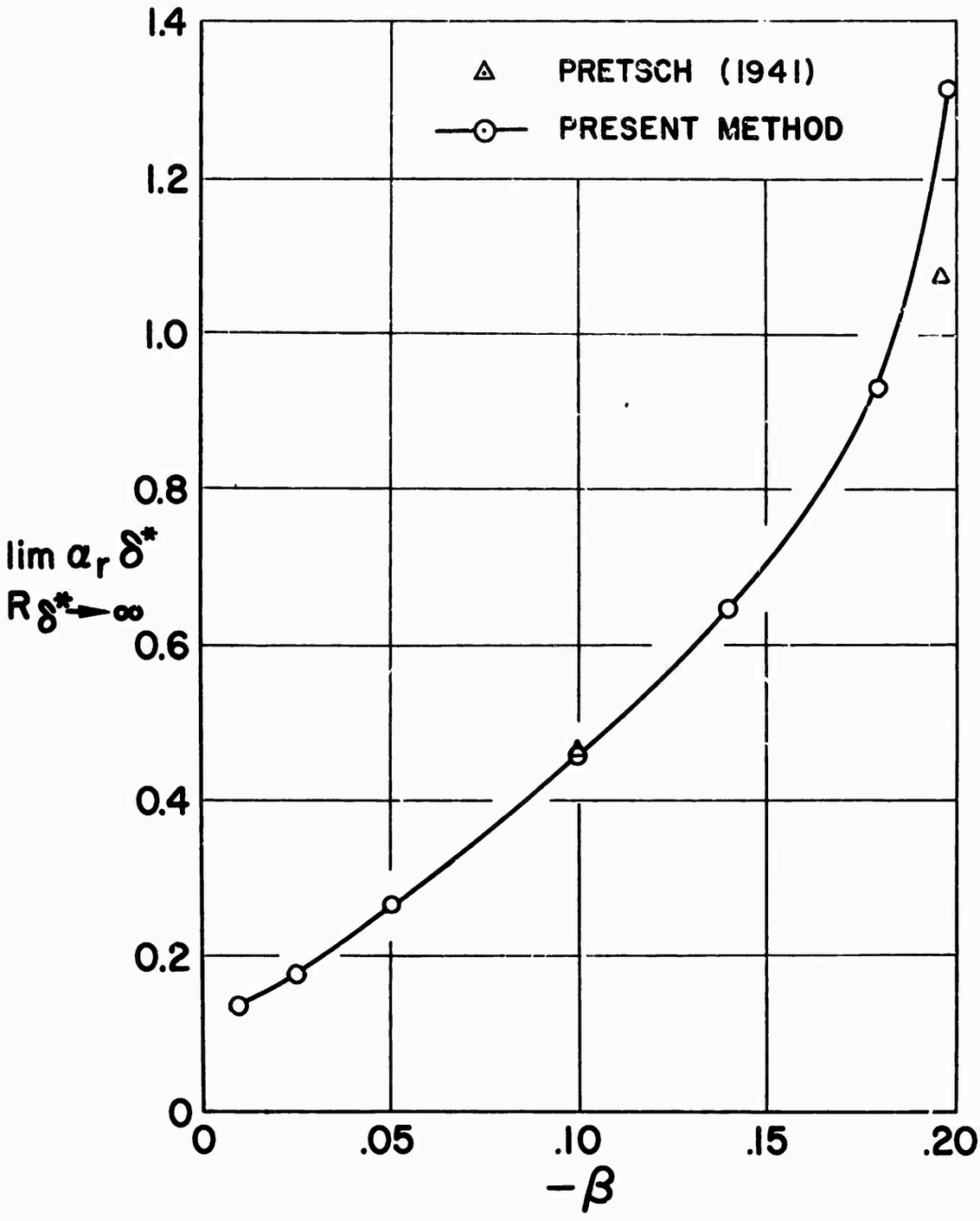

Figure 34. - The effect of adverse pressure gradient on the amplified wave-number spectrum in the inviscid region

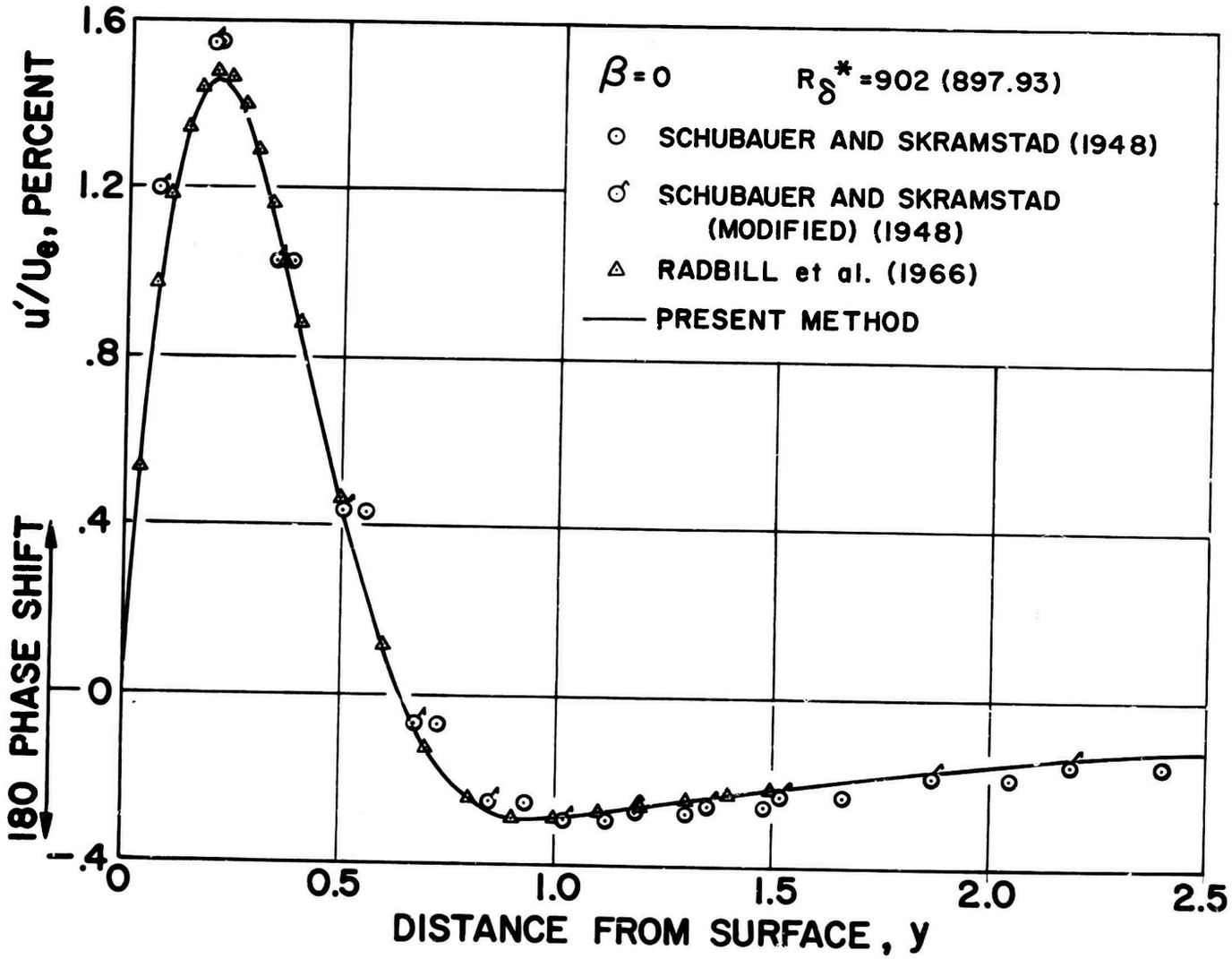

Figure 35. - Comparison of root-mean-square longitudinal disturbance velocity with data of Schubauer and Skramstad (R_{δ^*} = 902)

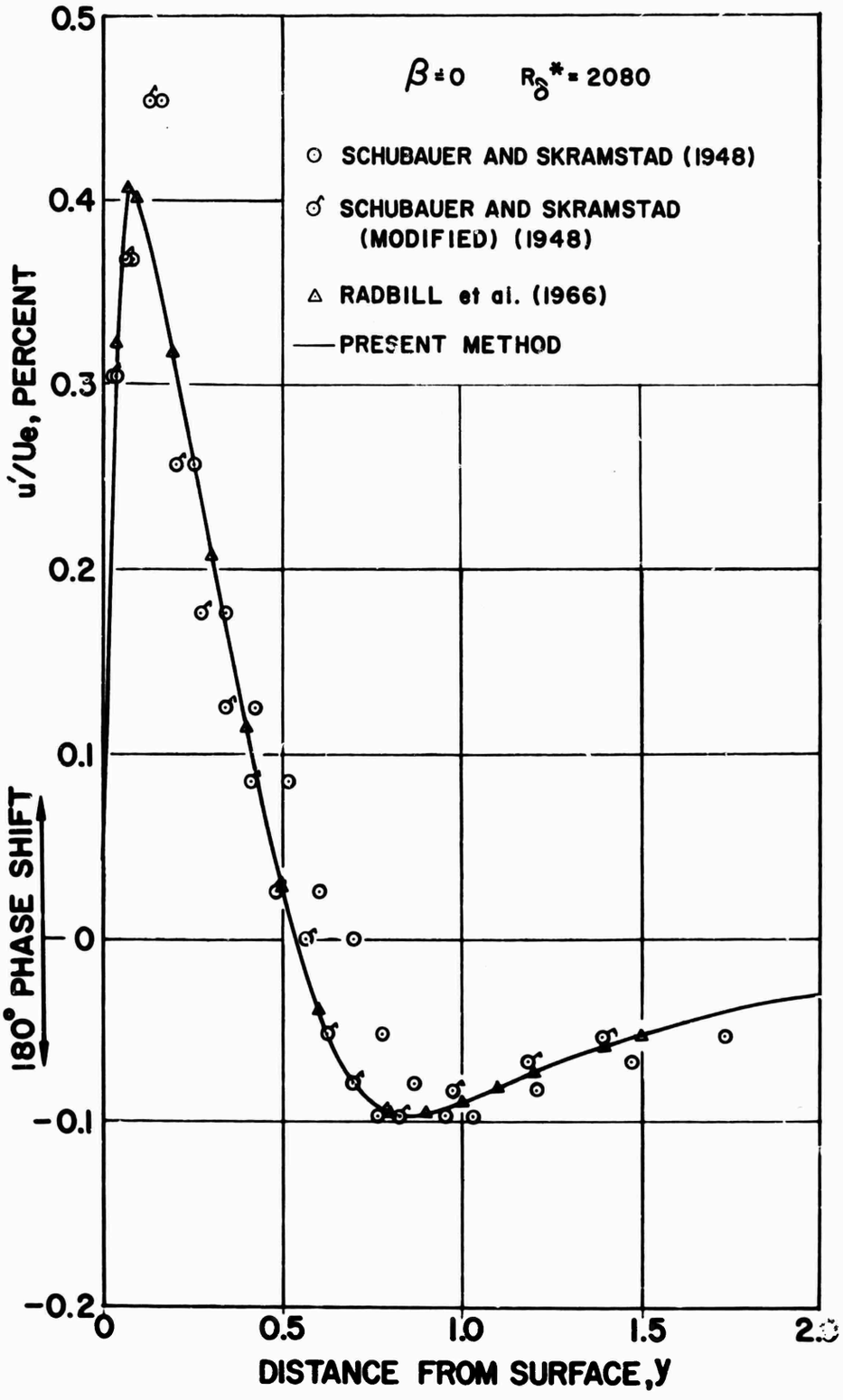

Figure 36. - Comparison of root-mean-square longitudinal disturbance velocity with data of Schubauer and Skramstad (R_{δ^*} = 2080)

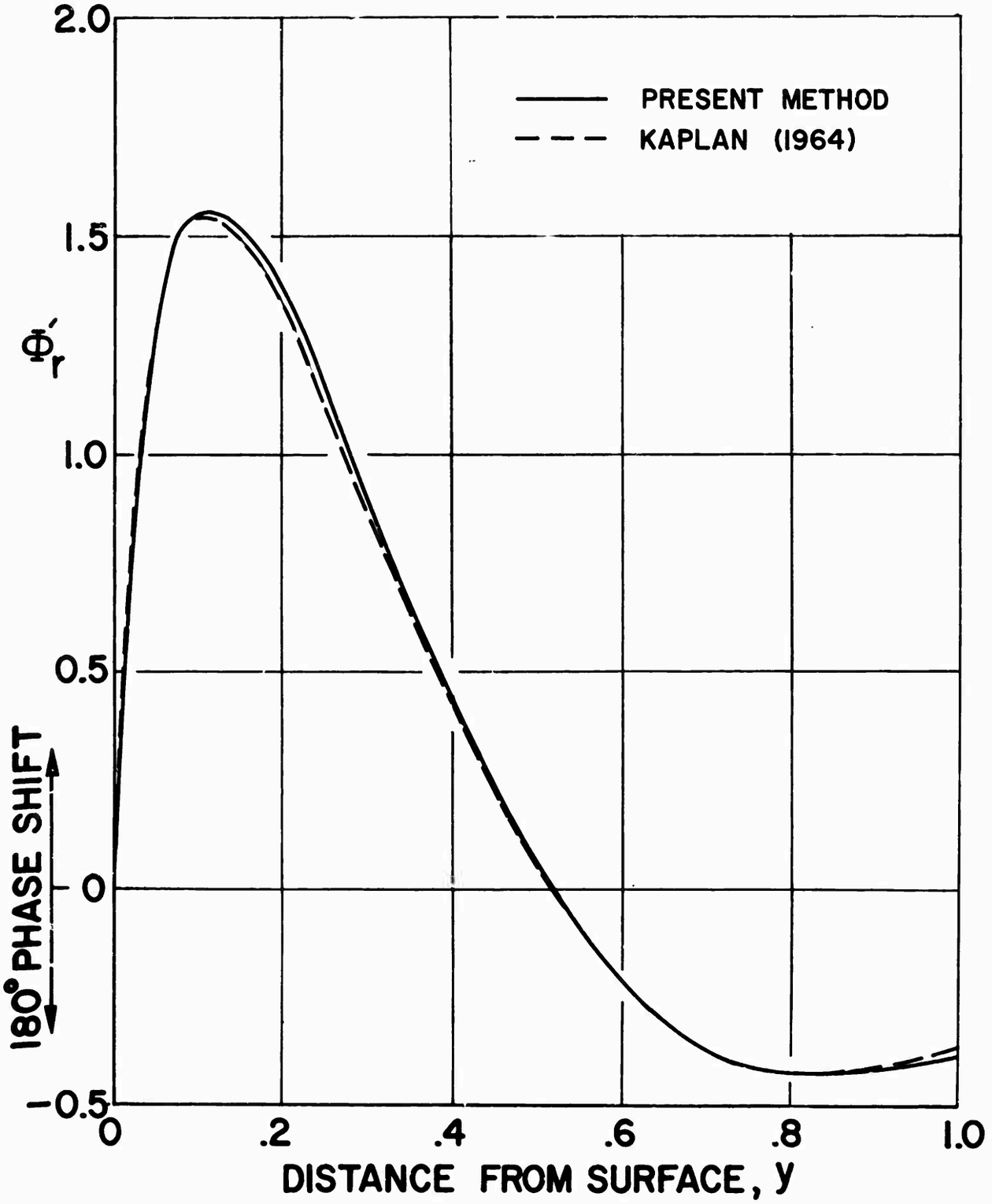

Figure 37. - Comparison of eigenfunction solutions with the results of Kaplan ($\beta = 0$, $R_\delta = 3000$)